geosciences

MDPI

Article

Ophiolitic Remnants from the Upper and Intermediate Structural Unit of the Attic-Cycladic Crystalline Belt (Aegean, Greece): Fingerprinting Geochemical Affinities of Magmatic Precursors

Christina Stouraiti [1,*], Iakovos Pantziris [1], Charalampos Vasilatos [1], Christos Kanellopoulos [1,2], Panagiotis Mitropoulos [1], Panagiotis Pomonis [1], Robert Moritz [2] and Massimo Chiaradia [2]

[1] Department of Geology and Geoenvironment, National and Kapodistrian University of Athens, Panepistimiopolis, Ano Ilissia, 15784 Athens, Greece; ipantziris@gmail.com (I.P.); vasilatos@geol.uoa.gr (C.V.); ckanellopoulos@gmail.com (C.K.); pmitrop@geol.uoa.gr (P.M.); ppomonis@geol.uoa.gr (P.P.)

[2] Department of Earth Sciences, University of Geneva, Rue des Maraîchers 13, 1205 Genève, GE, Switzerland; Robert.Moritz@unige.ch (R.M.); Massimo.Chiaradia@unige.ch (M.C.)

* Correspondence: chstouraiti@geol.uoa.gr; Tel.: +30-210-7274941; Fax: +30-210-7274063

Academic Editors: Basilios Tsikouras, Antonio Acosta-Vigil and Jesus Martinez-Frias
Received: 21 November 2016; Accepted: 7 March 2017; Published: 21 March 2017

Abstract: The ophiolitic rocks of the Attic-Cycladic crystalline belt are considered of key importance for understanding the Mesozoic tectonic evolution of the Aegean region. Unresolved questions concern their tectono-stratigraphic relationships across the region. The mode of occurrence of the Cycladic ophiolites varies, as they appear as: (a) dismembered blocks (olistoliths) within the supra-detachment units of Paros and Naxos; (b) mélange formations in the upper structural unit of western Samos and Skyros; and (c) meta-ophiolitic mélange in the Cycladic Blueschist Unit (CBU) from central Samos. The trace element geochemistry and Pb-Sr-Nd isotopes of the mafic ophiolitic rocks indicate four geochemical groups: (a) the upper unit metabasites from Paros and western Samos (Kallithea) display an evolved basaltic composition (Mg# 40.2–59.6), with low Zr/Nb values (5–16) and high Ce/Y values (1.3 to 2.6) compared to MORB, indicating island-arc tholeiite affinities; (b) Naxos upper unit metabasalts show spider diagrams patterns indicating ocean island basalt (OIB-type) affinities; (c) Central Samos metagabbros (CBU) are primitive rocks with Back-Arc Basin basalt affinities; (d) the Skyros metadolerites and Tinos (Mt Tsiknias) and S. Evia (CBU) metagabbros, cluster as a separate geochemical group; they exhibit high MgO values (>10 wt %), very low TiO_2 values (0.1–0.2 wt %), Y and Yb, and depleted trace element N-MORB normalized patterns, similar to volcanic rocks formed in modern oceanic fore-arc settings, such as boninites. A combination of the Pb- and Sr-isotopic compositions of Cycladic metabasites indicate that the Pb and Sr incorporated in the Cycladic ophiolites correspond to mixtures of magmatic fluids with seawater ($^{206}Pb/^{204}Pb$ = 18.51–18.80; $^{207}Pb/^{204}Pb$ = 15.59–15.7; $^{208}Pb/^{204}Pb$ = 39.03–39.80 and initial $^{87}Sr/^{86}Sr80$ = 0.705–0.707). Furthermore, peridotite relicts from Samos, Paros, and Naxos—irrespective of the structural unit—display chemical affinities of ocean floor peridotites formed in a supra-subduction zone. The characteristics of harzburgite relicts in Cycladic serpentinites and Skyros indicate a highly residual nature of the mantle source. Geochemical data from this study shed further light on the complex structure of the oceanic lithosphere from which the Cycladic ophiolites originated.

Keywords: Aegean ophiolites; Sr-Nd-Pb isotopes; MORB, BABB; supra-subduction zone

1. Introduction

Ophiolitic remnants are widespread in the Cyclades, southern Aegean, occurring in the upper portion of the tectono-stratigraphic stack (Figure 1) [1–6]. The mode of occurrence of ophiolitic associations varies in different parts of the Cyclades (Figure 1b,c) [7–9]. The typical mode of occurrence is within low-pressure metamorphosed mélanges in the Upper Cycladic Unit, as on the islands of Anafi [5], Ikaria [10], and Samos (Kallithea nappe) [11], interpreted as subduction–accretion units of Cretaceous age [12] (Figure 1c). In contrast to that is the centrl Cyclades ophiolitic upper unit, which is limited to the occurrence of serpentinized peridotites and minor mafic lithotypes [4]. In the central Cyclades islands of Paros and Naxos, supra-detachment basins associated with metamorphic core complexes enclose olistoliths of the latter lithologies overlain by Miocene and Pliocene sedimentary rocks [12,13]. Additionally, highly sheared serpentinites at the base of these basins mark the low angle detachment faults of Naxos-Paros, and their tectonic position is interpreted as representing a very weak horizon during progressive exhumation [14] (Figure 1c,d).

The initial age of formation of ophiolitic rocks of the upper unit of the central Cyclades is unknown, although in other Cycladic islands and Crete both Jurassic and Cretaceous age ophiolitic rocks have been reported [5,10,15]. Additionally, dismembered metaophiolites occur in the intermediate structural unit enclosed as blocks within mafic mélange units of the Cycladic Blueschists Unit (CBU) [4,6,15–17] (Figure 1b). Based on the geochemical characteristics and structural appearance, these metaophiolitic rocks in the Cycladic islands (e.g., Samos, Syros, Tinos: [15]) have been correlated to the Jurassic ophiolites of the Pindos basin (western ophiolite belts) [5]. An important question arising is whether the late Cretaceous ophiolite remnants from some Cycladic Upper Unit occurrences were high-level parts of a long (~25 Ma) accretion–subduction process of which the Eocene blueschist ophiolite remnants are deep-level representatives [4].

In the Hellenides orogenic belt a major Tethyan-type ophiolite emplacement occurred in mid- to late Jurassic times [18]. This ophiolite belt ('Eohellenic' ophiolites) is interpreted as originating from a Mesozoic Neo Tethyan oceanic basin, the Pindos Ocean, and subsequently thrust northeastwards onto the Pelagonian passive continental margin (Figure 1; [19,20]). Ophiolite remnants in the upper structural units of the Cycladic islands and Crete have been considered as the southernmost continuation of this belt, based mainly on their tectonic position and geochemical characteristics [5] (Figure 1b). However, it is not yet well understood whether all the Cycladic ophiolites correlate with the Middle Jurassic ophiolites of the Pindos ocean ("Eohellenic nappe") in western Greece [21], or if some occurrences correlate with the Upper Cretaceous (70–95 Ma) ophiolites of western Turkey, and Cyprus [18]. Ophiolite rocks from a mélange formation of Skyros and other northern Aegean islands are interpreted, according to their tectonic position, as possible Cretaceous age obducted ophiolite from the internal Vardar ocean [5,22].

Based on their tectonic setting, an ophiolite is emplaced either from down-going oceanic lithosphere via subduction–accretion, or from the upper plate in a subduction zone through trench–continent collision [23,24]. In the case of the Aegean ophiolites, both modes of emplacement occur, indicating a change of the tectonic setting in the Aegean region through the Mesozoic time [25–29].

In this paper, we examine in detail the chemical compositions of mafic and associated ultramafic rocks from the structurally upper unit of Paros-Naxos, Samos, and Skyros, as well as minor occurrences of metamafic rocks from the migmatitic gneiss dome of Naxos (Figure 2). Moreover, we make a comprehensive overview of published geochemical data of ophiolitic lithologies from typical ophiolite exposures of the upper structural unit (UU) of Tinos [15] and Ikaria [10], and compare them with the metamorphosed ophiolitic mélange units (CBU) from Tinos, southern Evia, Andros, Samos [4,15,28], and Naxos [29], in order to place the new data into a regional context.

With these new whole-rock geochemical data that include Sr-Nd-Pb isotopic data for metabasites and ultramafics, we aim to: (a) present a basic geochemical characterization from the ophiolite occurrences of different Aegean islands (Cycladic islands and Skyros); and (b) recognize distinguishing chemical characteristics in order to make regional correlations.

This research paper is based on sampling and whole-rock (major and trace element) analytical data collected by [30] and augmented later on by isotopic data on selected rock samples.

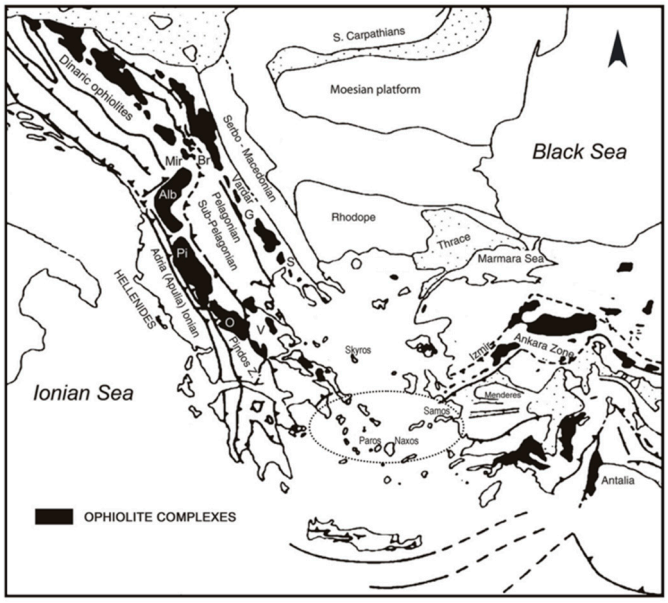

(**a**)

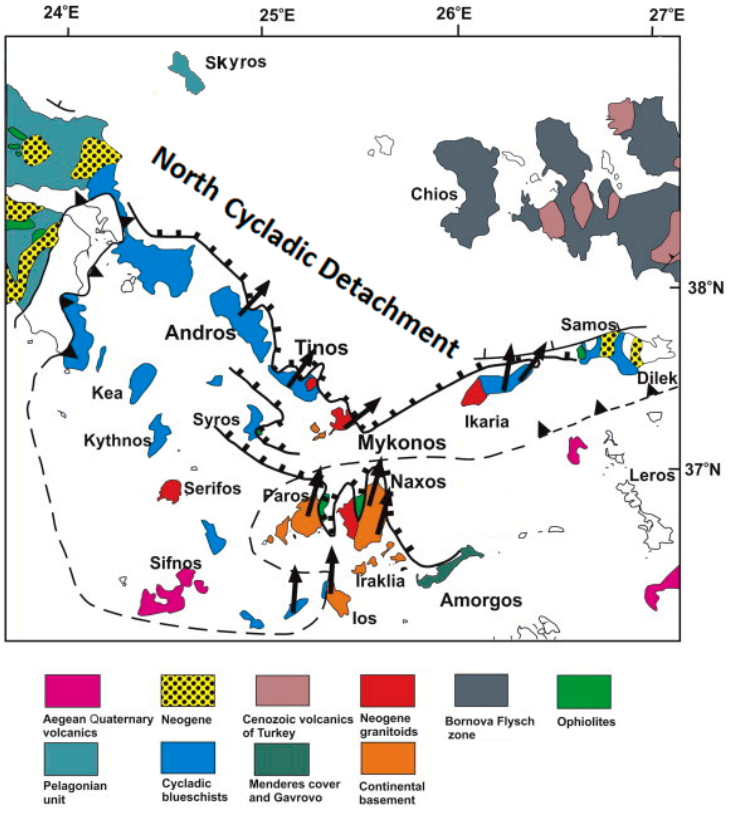

(**b**)

Figure 1. *Cont.*

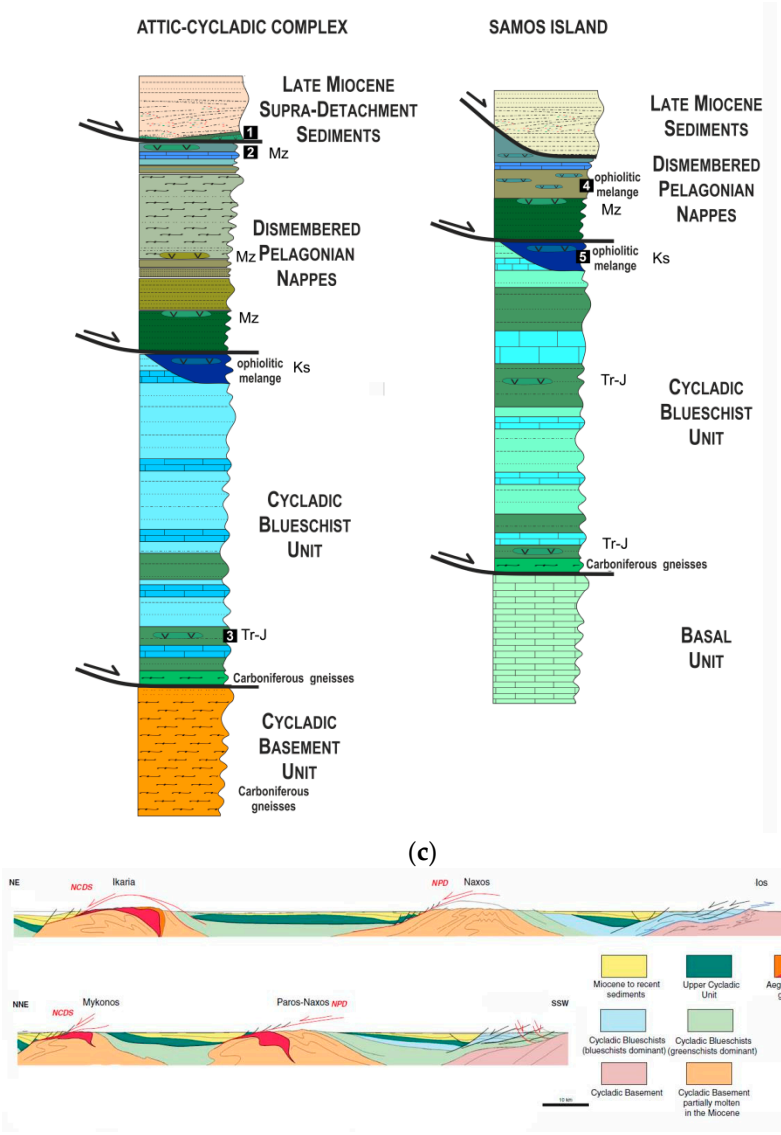

Figure 1. (**a**) Distribution of Mesozoic ophiolite complexes in the Hellenides and its northward and eastward continuation in the Dinarides and the Taurides, respectively. The tectonic sketch map is modified after [7,8]. Abbreviations: Alb = Albanian, BR = Brezovica, G = Guevgueli, Mir = Mirdita (Albania), O = Othris, Pi = Pindos, S = Sithonia, V = Vourinos. (**b**) Simplified geological map of the Attic-Cycladic Crystalline Belt, showing the major tectonic units. Distribution of the Cycladic Blueschist Unit (CBU), the Cycladic Basement rocks, and the Pelagonian unit within the ACC is also shown (modified after [12] and references therein). (**c**) Schematic tectono-stratigraphic sequence of the main Cycladic units after [1,12–14] and Samos nappe piles after [19,26]. The stratigraphic location of the ophiolitic rocks is marked with numbers on the columns: 1—Naxos and Paros dismembered supra-detachment ophiolites; 2—Skyros melange; 3—Naxos amphibolites from the CBU; 4—western Samos (Kallithea) mélange; 5—central Samos meta-ophiolitic mélange (CBU). Age abbreviations: Mz—Mesozoic, Ks—Cretaceous; Tr-J—Triassic-Jurassic. (**d**) Structural cross-sections across the Cycladic metamorphic belt showing the main structural units and the location of ophiolitic rocks, modified after [9].

2. Geological Setting

Earlier studies in the Attic-Cycladic crystalline belt (Figure 1b) have described two main structural units with different tectono-metamorphic histories (e.g., [1,2,31]). The Upper Unit (or Upper Cycladic Unit) forms the hanging-wall to the Cycladic extensional detachments. It consists of a heterogeneous sequence of Permian to Tertiary sediments, Mesozoic ophiolites (Figure 1c) and pre-Eocene metamorphic rocks transgressively covered by Late Cretaceous unmetamorphosed carbonates, as well as Late Cretaceous medium-pressure/high-temperature rocks and granitoids (e.g., [3,9,32,33]. This upper unit contains mélanges with metaigneous blocks and tectonic slabs (ranging from 1 m to several hundred meters long) that are enclosed in an ultramafic or metasedimentary matrix (e.g., [17,31,34]).

The structurally intermediate unit is equivalent to the Cycladic Blueschist Unit (CBU), which is the dominant tectonic unit in the Cyclades. The CBU consists of remnants of pre-Alpine crystalline basement and a stack of tectonic subunits comprised of a metamorphosed volcano–sedimentary succession (e.g., [31]). The CBU underwent regional eclogite- and blueschist-facies metamorphism during Late Cretaceous to Eocene compression (M1 metamorphic event) [18,35,36]. The Blueschist facies event was followed by a late Oligocene–Miocene, mostly greenschist-facies overprint (M2) with peak conditions of ~450–500 °C and 4–9 kbar [2,35]. In Paros and Naxos M2 reached amphibolite-facies conditions (e.g., [37]). The CBU is considered equivalent to the Pindos zone and to rocks directly underlying the Pelagonian basement.

In the CBU there are widespread tectonic slices of ophiolites, intercalated with marbles, metapelites, mafic volcanites and flysch [3]. These exposures include the metamorphic rocks in Andros, Tinos, Sifnos, Syros, Naxos and, further north, the Lavrion Blueschist Unit [38] and the Styra-Ochi unit of southern Evia [34]. In most studies these units are considered equivalents of the Pindos ocean and some are correlative with sub-ophiolitic mélanges (Figure 1b).

The age of meta-ophiolitic fragments (olistoliths) from the Upper Unit of the Attic-Cycladic crystalline belt and the Late Miocene supra-detachment sedimentary units is considered to be pre-Late Cretaceous according to the Cretaceous metamorphic ages of those units [32,33]. However, an overview of published radiometric data by [39] indicates that both Jurassic and Cretaceous meta-ophiolites occur in the HP mélanges of the CBU, but it is still questionable whether those age groups occur within the same mélange formations or at different lithostratigraphic and/or tectonic levels (Figure 1c).

2.1. Local Geology

On Paros, ophiolitic rocks occur in the Marmara nappe, which in places are transgressively covered by Barremian age limestones (Figure 1c). This transgression is considered to represent the timing of emplacement of ophiolites from the Pindos ocean over the Pelagonian continental margins (Eohellenic event) [40]. The lower part of the Marmara Nappe (Supra-detachment units of map, Eastern Paros in Figure 2a), consists mainly of serpentinites, which preserve relicts of peridotite and only minor blocks of metabasites (metagabbros, Figure 2a).

On Naxos, mafic-ultramafic rock associations from the Upper unit occur as: (a) blocks and slabs of variable size (hundreds of meters) of serpentinized peridotites containing lenses of metagabbros (Galanados, Figure 2b); (b) small occurrences of metagabbros found along the detachment plane; and (c) slices of brecciated metadolerites enclosed in a matrix of sandstone, conglomerate and chert (Agios Thaleleos, Figure 2b). Additionally, metamorphosed and foliated ultramafic rocks mark the contact between the upper and lower structural units [16]. These metamorphosed ultramafic rocks occur as elongated bodies, and often they are marked by the formation of monomineralic zones at their contact with the surrounding gneisses and schists. Serpentinites from two stratigraphic horizons are sampled in this study: (a) the main horizon of meta-ultrabasic bodies of Naxos dome at the boundary of leucogneiss-core with the Lower Series [29], from the localities of Agia and Kourounohori; and (b) the Upper (supra-detachment) Unit serpentinites from the localities of Galanados and Agios Thaleleos (Figure 2b). The aim was to evaluate the similarities/differences between samples from different structural units of the same islands.

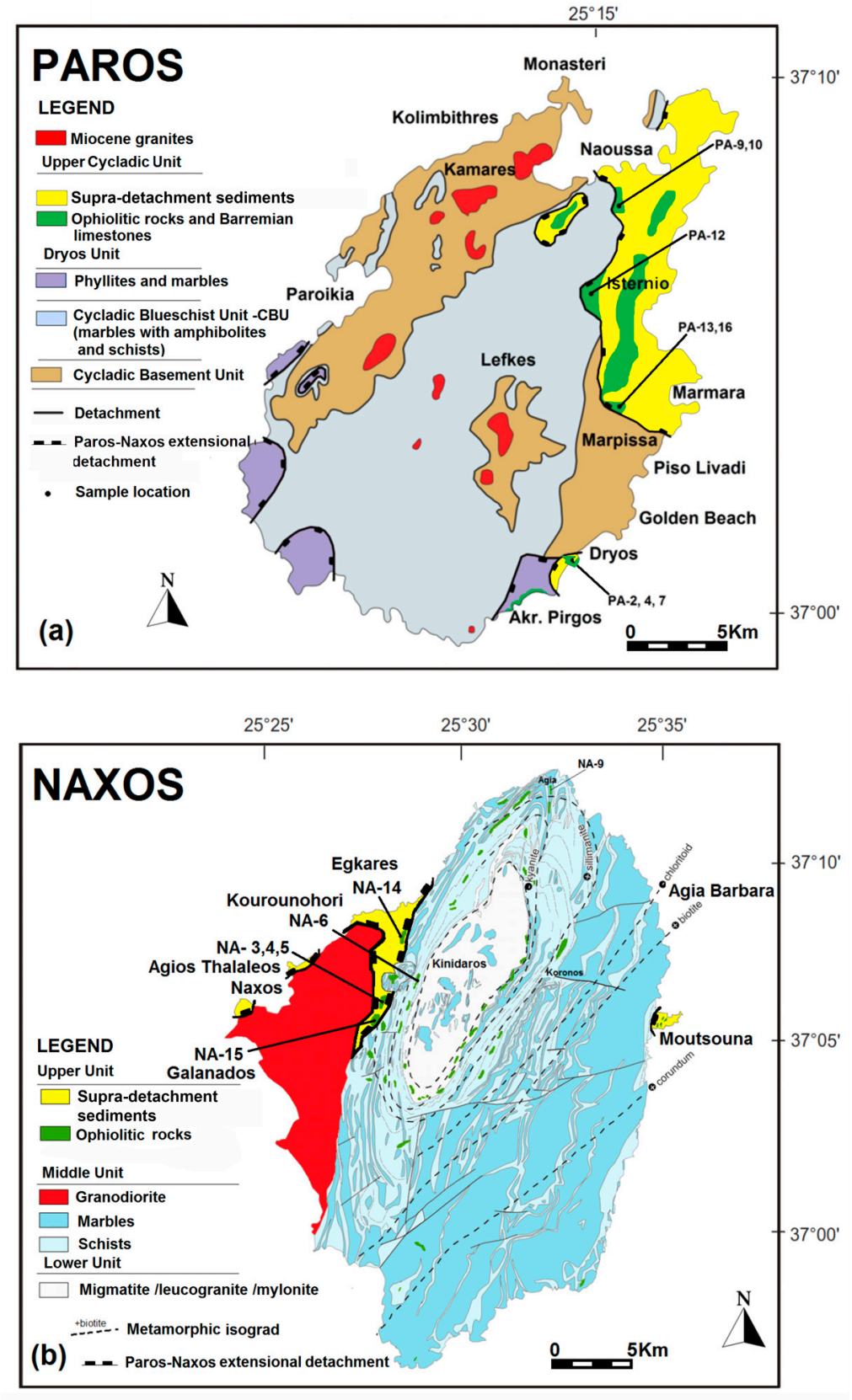

Figure 2. *Cont.*

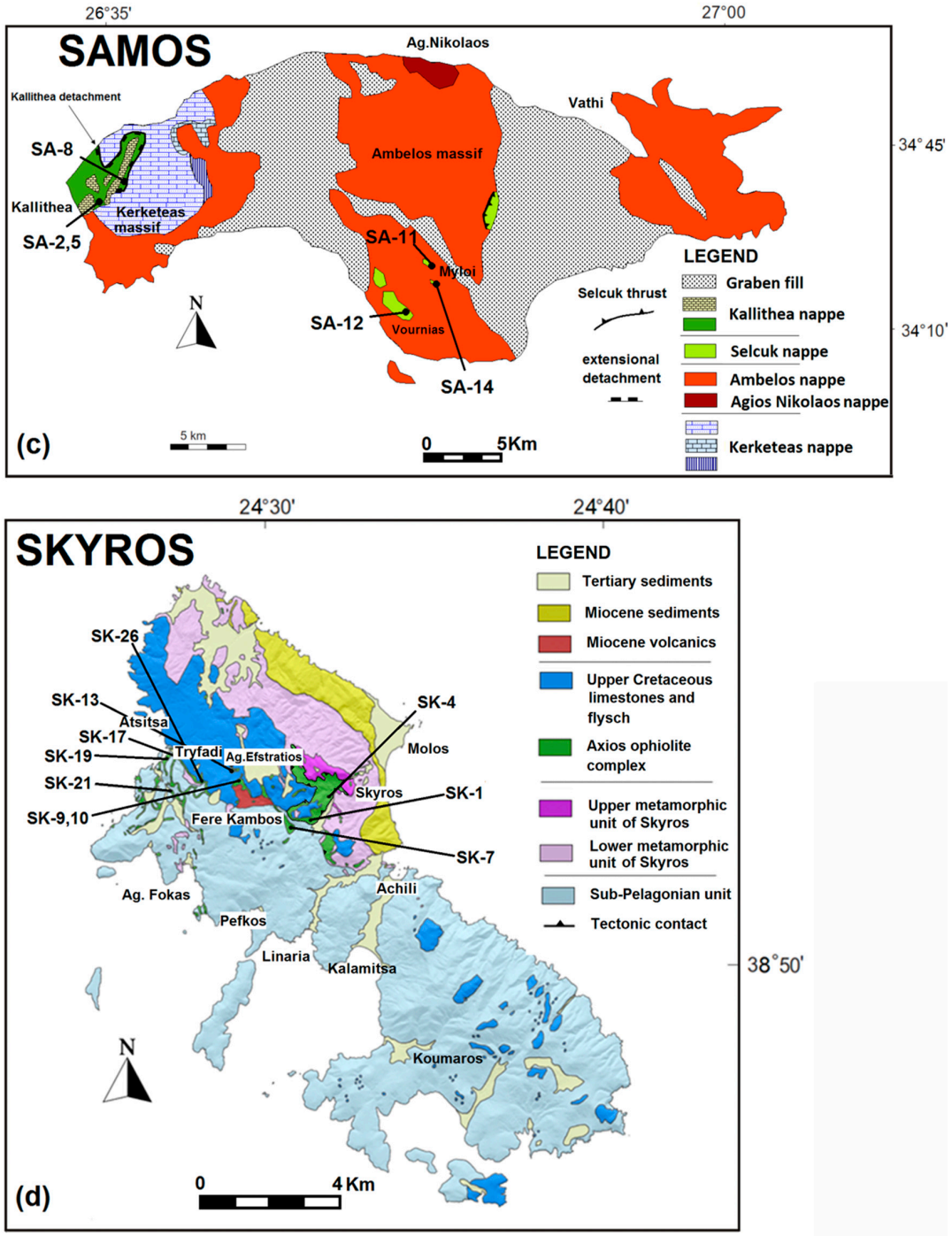

Figure 2. Detailed geological maps of the (**a**) Paros (after [14]); (**b**) Naxos by [8,25]; detailed geological maps of the (**c**) Samos (modified after [26,40]); (**d**) Skyros by [27]). Numbers indicate sample locations.

On Samos island six subunits have been distinguished by previous authors (Figures 1c and 2c). These include the metamorphosed Selçuk, Ampelos, Agios Nikolaos, and Kerketas nappes, and the uppermost Kallithea nappe in western Samos [26,40], Figure 2c. An ophiolitic mélange has been described at the uppermost unit of Kallithea nappe (western Samos, Figure 2c). This unit is described as chaotic mixture of pillow basalts, relict peridotites, serpentinites, conglomerates, radiolarites, clastic sediments, and limestones containing ammonitico rosso, having a thickness of 200 to 300 m [11]. The size of mafic and ultramafic blocks within this chaotic formation ranges from few centimeters to

tens of meters. Moreover, a metamorphosed mélange is described in the Selçuk nappe, at central Samos (Figure 2c). The Selçuk nappe has been correlated to the upper most part of the Cycladic Blueschist Unit [40]. For the purpose of this study we have sampled ophiolitic occurrences from the Upper Unit (Kallithea nappe) as well as central Samos metaophiolitic mélange.

On Skyros island, central Aegean (Figure 2d), an ophiolitic mélange overthrusts the Palaeozoic–Middle Jurassic Pelagonian basement rocks and is considered as part of the Eohellenic nappe [5]. K-Ar dating on a gabbroic rock (diorite) from Skyros mélange determined a Lower Cretaceous age (125 ± 8 Ma), which has been assigned to the formation age of the magmatic protolith [5]. Ophiolite lithologies outcrop in the central–northern part of the island (Figure 2d) and consist of highly deformed serpentinite, massive gabbroic rocks, dolerite dykes, and massive basaltic/andesitic lavas and ophicalcite [41]. In the framework of this study, selected mafic and ultramafic rocks from the Skyros mélange are compared with the structurally correlative Upper Cycladic Unit ophiolitic rocks.

3. Analytical Techniques

Thirty-three rock samples (13 metabasites and 20 serpentinites) were analyzed for major and trace elements. Sample locations are provided in Supplementary Table S1. Of these, 11 samples—selected as representative for each lithological type—were analyzed for Sr and Nd isotope compositions. Lead isotope ratios were measured on representative samples from Naxos, Paros, and Samos metabasic rocks. Lead isotope analyses of the metaperidotites samples were not possible to be determined due to the very low U and Pb concentrations in these samples, except for two samples from Naxos (NA-6, NA-14).

Major and trace element concentrations of the rock samples were determined by the XRF technique at Leicester University (UK). Major elements were determined on glass beads fused in a gold–platinum crucible at 1100 °C from ignited powders, and trace elements were determined on pressed powder pellets (see Supplementary Materials). Major elements were determined using Rh anode excitation, and the trace elements Sc, V, Cr, Ni, Zn, Ga, Rb, Sr, Y, Zr, Nb, La, Ce, Nd, and Ba, on pressed powder briquettes, using either Rh or W excitation, both on the Phillips PW1600 X-ray fluorescence spectrometer (Phillips electronics, Eindhoven, The Netherlands). Details of operating conditions and techniques for this instrument are given in [42]. Although the concentrations of some of the trace elements (particularly Nb, La, Ce, and Th) were near or below the limit of detection by XRF techniques in many samples, a number of key, relatively immobile, elements were able to be determined with sufficiently high precision by XRF methods to enable clear deductions concerning the petrogenesis of the Cycladic ophiolitic rocks.

Radiogenic isotopic compositions of Sr, Nd and Pb were measured on 12 whole rock (six metaperidotite and six metabasites) samples from Naxos, Paros, Samos, and Skyros at the University of Geneva, Switzerland. Between 100 and 120 mg of whole rock powder were dissolved during seven days in Savillex® Teflon (Savillex, Minnetonka, MN, USA) vials using 4 mL of concentrated HF and 1 mL of HNO_3 14 M, at a temperature of 140 °C and with the help of ultrasonication for 30 min twice a day. Subsequently, samples were dried and re-dissolved for three days (also with 30 min ultrasonication twice a day) in 3 mL of HNO_3 14 M, and dried again. Sr, Nd, and Pb were then separated using cascade columns with Sr-Spec, TRU-Spec, and Ln-Spec resins, respectively, according to a protocol modified from [43]. Finally, the material was redissolved in 2% HNO_3 solutions and ratios were measured using a Thermo Neptune PLUS Multi-Collector ICP-MS (Thermo Fisher Scientific, Waltham, MA, USA) in static mode. Ratios used to monitor internal fractionation were: $^{88}Sr/^{86}Sr$ = 8.375209 for the $^{87}Sr/^{86}Sr$ ratio, $^{146}Nd/^{144}Nd$ = 0.7219 for the $^{143}Nd/^{144}Nd$ ratio, and $^{203}Tl/^{205}Tl$ = 0.418922 for the three Pb ratios (a Tl standard was added to the solution). External standards used were SRM987 ($^{87}Sr/^{86}Sr$ = 0.710248, long-term external reproducibility: 10 ppm), JNdi-1 ($^{143}Nd/^{144}Nd$ = 0.512115; [44] long-term external reproducibility: 10 ppm), and SRM981 [45] for Pb (long-term external reproducibility of 0.0048% for $^{206}Pb/^{204}Pb$, 0.0049% for $^{207}Pb/^{204}Pb$ and 0.0062% for $^{208}Pb/^{204}Pb$). $^{87}Sr/^{86}Sr$, $^{143}Nd/^{144}Nd$ and Pb isotope ratios were further corrected for external fractionation (due to systematic differences between measured

isotope ratios and those proposed for SRM987, JNdi-1 and SRM981, by [44–46] respectively]) by −0.039‰, +0.047‰ and +0.5‰ amu, respectively. Interferences at masses 84 (^{84}Kr), 86 (^{86}Kr) and 87 (^{87}Rb) were corrected by monitoring ^{83}Kr and ^{85}Rb, ^{144}Sm interference on ^{144}Nd was monitored on the mass ^{147}Sm and corrected by using a ^{144}Sm/^{147}Sm value of 0.206700, and ^{204}Hg interference on ^{204}Pb was corrected by monitoring ^{202}Hg.

All the analyzed metabasites have low U/Pb (ranging from 0.1 to 0.5) as well as Th/Pb ratios, and therefore no corrections due to time-integrated decay of U and Th were made because the addition of radiogenic lead is considered to be insignificant (Table 1). An exception to this is Naxos metabasite NA-3, which displays an elevated Th/Pb value of 1.3, and the serpentinite NA-14, which is characterized by slightly more radiogenic compositions, suggesting a higher U/Pb ratio.

Table 1. Whole-rock major and trace element compositions of metabasites and ultramafic rocks from the Aegean ophiolites.

SAMPLE	NA-3	NA-4	NA-5	NA-7	NA-9	NA-15	PA-9	PA-10	SA-2	SA-5
Rock Type wt %	**Meta Basalt (UU)**	**Meta Basalt/ Andesite (UU)**	**Meta Basalt/ Andesite (UU)**	**Amphi-Bolite (CBU)**	**Amphi-Bolite (CBU)**	**Meta Gabbro (UU)**	**Meta Gabbro (UU)**	**Meta Gabbro (UU)**	**Meta Basalt (UU)**	**Meta Basalt (UU)**
SiO_2	42.00	53.49	54.53	50.21	56.6	45.94	50.41	52.19	38.88	49.04
TiO_2	1.79	1.41	0.35	0.21	0.10	1.40	0.61	0.51	0.69	1.92
Al_2O_3	17.11	13.19	12.75	7.33	3.56	15.00	14.36	16.36	15.99	17.01
Fe_2O_{3T}	9.59	8.62	4.75	5.59	7.51	8.89	7.75	7.49	8.57	11.17
MnO	0.14	0.14	0.16	0.07	0.29	0.10	0.15	0.17	0.12	0.12
MgO	3.26	5.27	2.30	25.87	19.17	4.66	5.21	4.54	6.39	3.39
CaO	11.4	11.07	10.06	6.09	12.20	11.55	11.05	11.03	12.99	4.62
Na_2O	2.14	1.06	1.24	0.08	0.17	3.20	1.99	2.79	2.18	6.44
K_2O	4.13	0.16	4.55	0.04	0.16	0.73	1.98	2.05	1.53	0.20
P_2O_5	0.49	0.25	0.10	0.01	0.01	0.54	0.17	0.42	0.13	0.01
LOI	8.27	5.78	9.20	5.21	1.46	7.48	6.51	2.60	12.69	6.76
TOTAL	100.32	100.44	100.00	100.71	100.22	99.49	100.21	100.57	100.15	100.72
Mg#	40.23	54.76	48.95	90.16	83.48	50.93	57.10	54.55	59.62	37.54
Trace elements (ppm)										
Sc	30	29	28	14	24	37	32	29	40	30
V	236	246	104	81	65	217	178	187	254	194
Cr	240	171	40	1212	1643	416	144	131	125	83
Co	45	42	21	57	71	46	34	33	34	30
Ni	130	90	32	1550	1035	225	42	45	40	32
Cu	10	50	39	bdl	4	49	88	42	18	3
Zn	100	67	55	37	144	64	95	73	57	77
Ga	19	16	11	8	6	14	13	15	15	15
Rb	79	2	142	bdl	8	15	56	62	39	22
Sr	206	395	204	12	33	216	299	262	152	231
Y	31	22	19	13	5	27	24	21	12	20
Zr	161	119	100	10	7	144	82	124	35	53
Nb	34	22	8	4	1	31	5	11	6	9
Ba	456	16	449	19	22	147	676	429	136	105
Pb	3	2	18	3	7	2	17	14	4	5
Th	4	2	11	2	bdl	4	3	9	2	3
U	1	1	2	1	1	1	2	2	bdl	1
La	19	17	21	4	bdl	24	11	32	11	15
Ce	47	29	37	3	2	39	30	54	16	28
Nd	26	16	19	6	2	20	14	23	8	11
Zr/Nb	4.7	5.4	12.5	2.5	7	4.6	16.4	11.2	5.8	5.9
Ce/Y	1.5	1.3	1.9	0.2	0.4	1.4	1.2	2.5	1.3	1.4
Nb/Y	1.09	1.0	0.42	0.3	0.2	1.14	0.2	0.52	0.5	0.45
SAMPLE	**SA-8**	**SA-11**	**SK-1**	**NA-6**	**NA-14**	**PA-2**	**PA-4**	**PA-7**	**PA-12**	**PA-13**
Rock Type wt %	**Meta Basalt (UU)**	**Meta Gabbro (CBU)**	**Meta Dolerite (UU)**	**Serp. Harzb. (CBU)**	**Serp. Harzb. (UU)**	**Harzb. (UU)**	**Harzb. (UU)**	**Harzb. (UU)**	**Harzb. (UU)**	**Harzb. (UU)**
SiO_2	46.06	44.93	50.35	43.13	40.66	39.86	40.71	39.93	41.80	39.76
TiO_2	0.68	1.04	0.13	0.04	0.01	0.02	0.02	0.02	0.05	0.01
Al_2O_3	16.74	18.80	16.70	1.74	0.9	1.44	1.66	1.43	2.68	0.85
Fe_2O_{3T}	8.57	8.01	4.24	8.47	8.86	8.15	8.26	7.87	8.37	7.91
MnO	0.14	0.15	0.06	0.13	0.07	0.07	0.07	0.06	0.13	0.10
MgO	6.29	9.09	10.04	42.58	36.76	36.29	36.98	37.15	34.12	37.60
CaO	10.21	11.61	12.82	1.61	0.76	0.13	0.06	0.04	1.99	0.97

Table 1. *Cont.*

SAMPLE	SA-8	SA-11	SK-1	NA-6	NA-14	PA-2	PA-4	PA-7	PA-12	PA-13
Rock Type wt %	Meta Basalt (UU)	Meta Gabbro (CBU)	Meta Dolerite (UU)	Serp. Harzb. (CBU)	Serp. Harzb. (UU)	Harzb. (UU)	Harzb. (UU)	Harzb. (UU)	Harzb. (UU)	Harzb. (UU)
Na_2O	1.18	1.73	1.47	bdl	bdl	0.27	0.03	0.04	bdl	bdl
K_2O	2.55	1.59	0.44	bdl	bdl	0.04	0.01	0.01	bdl	bdl
P_2O_5	0.18	0.24	0.01	0.09	0.07	bdl	bdl	bdl	0.01	0.01
LOI	7.54	3.47	3.60	1.66	11.86	12.59	12.31	12.37	10.96	13.33
TOTAL	100.15	100.55	99.87	99.45	99.95	98.87	100.11	98.94	100.05	100.47
Mg#	59.24	69.20	82.42	90.87	89.15	89.81	89.86	90.33	88.97	90.39
Trace elements (ppm)										
Sc	27	27	39	8	6	4	8	8	9	5
V	172	224	168	50	37	27	41	44	60	39
Cr	261	162	1159	2895	3932	1935	2634	2799	2525	1789
Co	35	43	36	100	112	63	88	81	95	95
Ni	72	244	210	2306	2312	2000	2564	2394	2119	2502
Cu	5	16	80	18	5	8	5	20	20	6
Zn	145	64	17	40	37	37	45	49	40	51
Ga	23	19	8	2	2	1	1	bdl	1	bdl
Rb	101	62	8	bdl	2	bdl	bdl	2	bdl	bdl
Sr	50	259	116	5	6	20	6	5	12	4
Y	12	30	5	bdl	1	1	1	2	2	1
Zr	67	100	20	bdl	bdl	bdl	bdl	2	2	bdl
Nb	55	2	<0.5	bdl	bdl	1	bdl	bdl	bdl	bdl
Ba	299	893	38	bdl	4	4	6	3	11	3
Pb	10	7	1	bdl	1	2	1	3	1	2
Th	3	bdl	bdl	bdl	bdl	bdl	bdl	bdl	bdl	bdl
U	1	1	1	bdl	1	bdl	1	1	1	3
La	10	2	2	bdl	bdl	bdl	3	bdl	2	bdl
Ce	27	8	5	bdl	bdl	bdl	bdl	bdl	bdl	bdl
Nd	13	8	3	bdl	bdl	bdl	bdl	bdl	2	bdl
Zr/Nb	13.4	50	50			1				
Ce/Y	2.25	0.26	1							
Nb/Y	4.58	0.06	0.08							

SAMPLE	PA-16	SA-12	SA-14	SK-4	SK-7	SK-9	SK-10	SK-13	SK-17	SK-19
Rock Type wt %	Harzb. (UU)	Olivin Pyrox. (CBU)	Olivin Pyrox. (CBU)	Harzb. (UU)	Harzb. (UU)	Lherz. (UU)	Harzb. (UU)	Harzb. (UU)	Harzb. (UU)	Harzb. (UU)
SiO_2	36.70	42.35	39.25	36.68	40.00	37.75	38.30	42.60	40.30	40.95
TiO_2	0.02	0.02	0.11	0.35	0.02	0.02	0.02	0.01	bdl	0.01
Al_2O_3	0.69	1.54	4.82	8.61	1.27	1.29	1.14	0.43	0.32	0.88
Fe_2O_{3T}	8.27	8.52	12.18	7.35	8.43	8.09	11.26	6.76	8.49	7.75
MnO	0.11	0.11	0.11	0.13	0.14	0.13	0.18	0.07	0.30	0.14
MgO	37.39	36.84	32.48	35.44	36.04	35.55	34.88	36.68	36.58	36.18
CaO	1.03	0.03	0.37	0.91	1.39	2.90	1.00	0.04	0.80	0.28
Na_2O	bdl	bdl	bdl	bdl	bdl	bdl	Bdl	bdl	bdl	bdl
K_2O	bdl	bdl	bdl	bdl	bdl	bdl	Bdl	bdl	bdl	bdl
P_2O_5	0.01	0.01	0.01	0.12	0.01	0.01	0.01	0.01	0.01	0.01
LOI	13.19	11.26	10.81	12.09	11.72	13.45	13.21	11.95	13.20	11.95
TOTAL	99.32	100.56	100.05	100.59	99.31	99.10	100.00	100.45	100.00	100.07
Mg#	89.95	90.02	84.07	90.52	89.43	89.69	85.98	91.48	89.51	90.24
Trace elements (ppm)										
Sc	4	4	7	6	6	13	33	3	7	34
V	7	34	87	90	45	49	32	16	36	5
Cr	3226	3367	2940	2014	2824	2542	2542	2213	3314	1578
Co	107	82	86	99	94	123	102	84	98	103
Ni	2720	2175	2218	1754	2285	2507	2375	2108	2452	2131
Cu	5	9	53	2	2	10	6	2	6	4
Zn	38	60	61	49	36	26	31	25	35	21
Ga	bdl	2	4	8	1	bdl	bdl	bdl	bdl	bdl
Rb	bdl	2	bdl	2	bdl	bdl	bdl	bdl	bdl	bdl
Sr	47	3	3	12	2	4	12	5	2	12
Y	1	4	3	7	1	2	1	1	bdl	1
Zr	bdl	2	3	82	bdl	2	bdl	bdl	bdl	bdl
Nb	bdl	bdl	bdl	6	bdl	bdl	1	bdl	bdl	bdl
Ba	3	bdl	7	3	4	5	11	22	bdl	18
Pb	1	1	1	3	1	2	1	1	3	2
Th	bdl	bdl	bdl	3	bdl	bdl	bdl	bdl	bdl	bdl
U	bdl	bdl	bdl	2	bdl	bdl	2	1	bdl	1
La	bdl	2	2	7	bdl	bdl	bdl	bdl	2	bdl
Ce	bdl	5	bdl	22	bdl	bdl	bdl	bdl	bdl	bdl
Nd	bdl	2	bdl	11	bdl	bdl	3	bdl	bdl	2
Zr/Nb				13.6			1			
Ce/Y		1.25		3.14						

Table 1. *Cont.*

SAMPLE	SK-21	SK-23	SK-26	Samos	Skyros	N-MORB	E-MORB	IAT [3]	OIB
Rock Type wt %	Olivin Webst. (UU)	Harzb. (UU)	Harzb. (UU)	Meta Gabbro [1] (CBU)	(SGBR) Meta Gabbro [2]				
SiO_2	39.83	40.59	38.68	49.90	50.37			51.03	
TiO_2	0.01	0.01	0.02	0.90	0.23	1.27	1.00	0.82	2.86
Al_2O_3	0.47	0.99	1.27	16.30	17.06			15.76	
Fe_2O_{3T}	9.00	7.49	10.19	6.40	5.67			11.76	
MnO	0.09	0.13	0.14	0.10	0.11			0.21	
MgO	30.72	38.86	37.45	8.00	9.00			6.30	
CaO	5.31	0.17	0.07	11.0	9.98			10.72	
Na_2O	bdl	bdl	bdl	3.60	2.80			2.40	
K_2O	bdl	bdl	bdl	0.50	0.81	0.072	0.25	0.18	1.44
P_2O_5	0.01	0.01	0.01	0.10	0.02	0.116	0.142	0.13	0.618
LOI	13.73	12.17	11.93	3.60	3.80				
TOTAL	99.06	100.31	99.67	100.40	99.96				
Mg#	87.11	91.13	87.92	71.28	76.06				
Trace elements (ppm)									
Sc	11	6	7	34.8	41				
V	19	37	44	207.3	177				
Cr	3359	2938	3104	366.7	520			100	
Co	100	87	105	27.3	31				
Ni	2388	2234	2826	151.7	111			14	
Cu	14	1	5	20	15				
Zn	19	33	32	40	7			79	
Ga	bdl	bdl	1						
Rb	bdl	bdl	bdl	15	11	0.6	5	3	31
Sr	21	1	1	179	193	90	155	133	660
Y	1	bdl	bdl	19	10	28	22	18	29
Zr	bdl	bdl	bdl	53	32	74	73	29	280
Nb	bdl	bdl	bdl	1.1	0.1	2.3	8.3	1	48
Ba	bdl	3	4	108	34	6.3	57	57	350
Pb	2	2	bdl	bdl	1.4	0.3	0.6		3.2
Th	bdl	bdl	bdl	0.1		0.1	0.6		4
U	1	bdl	bdl	0.1	0.1		0.2		1
La	bdl	bdl	bdl	2.5	1.4	2.5	6.3	1.59	37
Ce	bdl	bdl	bdl	7	2.3	7.5	15	4.99	80
Nd	bdl	bdl	bdl	6.6	1.4	7.3	9	4.39	38.5
Yb				1.76	1.22	3.1	2.4	1.84	2.2
Ce_N/Yb_N				1.04	0.49	0.63	1.64	0.71	9.55
Zr/Nb				48.1	320	32.2	8.8	29	5.8
Ce/Y				3.14	0.2	0.2	0.7	0.3	2.7
Nb/Y				2.8	3.2	2.6	3.3	1.6	9.7

bdl.: Below the detection limit (see Supplementary Material for detection limits). Total iron given as Fe_2O_{3T} and LOI is loss on ignition. Mg# = 100*MgO/(MgO + FeOt) with oxides in molar proportions. Mg# calculated for all samples on anhydrous basis. Locations: NA—Naxos. PA—Paros. SA—Samos. SK—Skyros. Rock type abbreviations: basalt/and.—basaltic andesites, Amphib.—Amphibolite; Harzb.—Harzburgite; Olivin Pyrox.—Pyroxenite; Lherz.—Lherzolite; Olivin Webst.—Websterite. [1] Central Samos metagabbros from CBU (n = 5), data from [15]; [2] Skyros metagabbro (SGBR), data from [41]; [3] IAT—Island Arc Tholeiite, South Sandwich island arc [47]. Ce_N/Yb_N normalized values to Chondrite CI and average elemental composition of MORB and OIB from [48].

4. Petrography

4.1. Naxos

The metaophiolitic outcrops of Naxos comprise mafic and ultramafic rocks. Mafic rocks are classified as (a) metagabbros and (b) metavolcanics. Ultramafic rocks comprise dunites and serpentinites.

4.1.1. Amphibolites

The metagabbros (CBU) are now amphibolites and display mainly granoblastic to lepidoblastic medium-grained textures, and occasionally relicts of igneous texture are preserved. They consist of 30–60 vol % amphibole, 20–30 vol % strongly altered plagioclase, 10–20 vol % chlorite, 15–20 vol % epidote, and accessory magnetite, quartz, and carbonates. Amphibole typically occurs as needles and slender prisms of actinolite, which locally display orientation. In places, slender prisms of actinolite and fibres of tremolite and chlorite surround porphyroblasts of relict plagioclase (NA-9, Figure 3a).

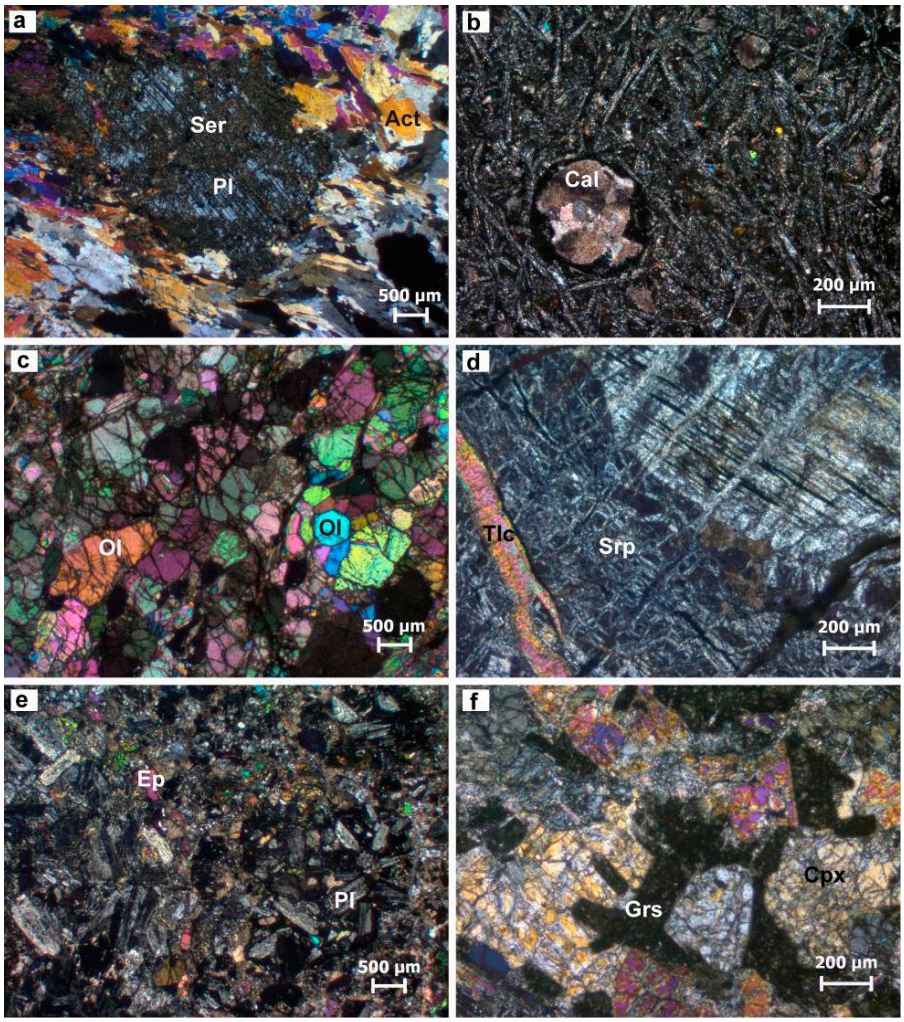

Figure 3. Photomicrographs (XPL) of: (**a**) sericitized plagioclase porphyroblast surrounded by slender prisms of actinolite (NA9 amphibolite, Naxos); (**b**) intersertal texture with amygdule filled with secondary calcite and iron oxides (NA3 spilite, Naxos); (**c**) equigranular polygonal olivine crystals forming a mosaic texture in dunite (NA6 dunite, Naxos); (**d**) mesh texture and bastite pseudomorph in serpentinite (PA12 serpentinite, Paros); (**e**) porphyritic intersertal texture in meta-andesite (SA8 meta-andesite, Samos); (**f**) blasto-subophitic texture in rodingite (SK1 rodingite, Skyros). (Act: Actinolite, Cal: Calcite, Cpx: Clinopyroxene, Ep: Epidote, Grs: Grossular, Ol: Olivine, Pl: Plagioclase, Ser: Sericite, Srp: Serpentine, Tlc: Talc).

Plagioclase laths are totally replaced by a cloudy microcrystalline aggregate of sericite, albite, calcite, epidote, and clinozoisite, forming pseudomorphs due to sericitization and saussuritization.

4.1.2. Metavolcanics

Metavolcanics of Naxos consist of spilites and metabasalts (prasinites). Spilites are characterized by relict intersertal, spherulitic, variolitic, and amygdaloidal texture, consisting of 50–70 vol % albite, 10–20 vol % chlorite, 5–10 vol % calcite, 5–10 vol % epidote, devitrified glass, and quartz. Spherulite shows radiating aggregates of acicular plagioclase altered to albite, while variolitic textures are fan-like altered plagioclase needles within glassy groundmass. Locally, rounded and elliptical amygdules that are 0.5–1 mm in diameter (Figure 3b), are filled mainly with calcite, while zeolite, epidote and secondary quartz are presented as minor constituents. Iron oxides, occurring in the groundmass and along fractures, are late magmatic minerals. Some late veins of quartz cut across the rocks.

Metabasalts show fine-grained granoblastic to lepidoblastic texture, consisting of clinozoisite, epidote, chlorite, albite, actinolite, white mica, calcite, titanite, and quartz. Late veinlets of quartz and feldspars crosscut the rocks.

4.1.3. Dunites and Serpentinites

Dunites show a rather constant mineralogical composition, comprising mainly of olivine with subordinate orthopyroxene and spinel. These fine-grained rocks display mosaic and fine equigranular textures composed of small, polygonal and occasionally unstrained olivine neoblasts (Figure 3c). Spinel is dark red and display anhedral grains heterogeneously distributed in the olivine matrix. Locally, spinel grains exhibit narrow rims of magnetite. The degree of serpentinization varies between 10% and 30%.

Serpentinites display in general mesh texture and consist essentially of serpentine minerals, mainly antigorite with minor chlorite, calcite and talc. The only preserved primary phase is Cr-spinel, which occasionally is totally replaced by magnetite. Pseudomorphic prismatic plates of bastite (lizardite pseudomorphs after pyroxenes), which sometimes mimic the cleavage of earlier pyroxene, are common.

4.2. Paros

The collected metaophiolitic mafic and ultramafic rock samples from Paros are classified as: (a) metagabbros and (b) serpentinites.

4.2.1. Metagabbros

The metagabbros display relict granular to granoblastic textures and consist of 30–40 vol % plagioclase, 20–30 vol % amphibole, 5–10 vol % chlorite, ~5 vol % epidote, minor titanite, and accessory magnetite, quartz, and carbonates. Plagioclase laths are replaced by a microcrystalline aggregate of sericite, albite, calcite, epidote and clinozoisite, forming pseudomorphs due to sericitization and saussuritization. Amphibole typically occurs as thin prisms and fibres of actinolite and tremolite, replacing clinopyroxene. Relicts of clinopyroxene occur as inclusions within some amphibole prisms, or more rarely as large xenomorphic crystals up to 5 mm in diameter, surrounded by continuous thin rings of actinolite and chlorite. These metagabbros show better preserved igneous textures relative to the amphibolites of Naxos, and have not acquired a visible metamorphic fabric.

4.2.2. Serpentinites

Serpentinites exhibit mesh and locally hourglass textures. They consist essentially of serpentine minerals, mainly antigorite with minor chlorite, calcite and talc. The only preserved primary phases are relicts of olivine and Cr-spinel, which occasionally is totally replaced by magnetite. Pseudomorphic prismatic plates of bastite (lizardite pseudomorphs after pyroxenes), which sometimes mimic the cleavage of earlier pyroxene, are common (Figure 3d). Sparsely, veinlets of calcite, magnesite and talk crosscut the serpentinites.

4.3. Samos

The ophiolitic rock samples from Samos are classified as: (a) metagabbros; (b) metavolcanics and (c) serpentinized harzburgites—serpentinites.

4.3.1. Metagabbros

Metagabbros are medium- to fine-grained rocks with poikiloblastic texture. They contain 15–35 vol % plagioclase, 10–20 vol % clinozoisite, 10–15 vol % clinopyroxene, 10–15 vol % amphibole, 5–10 vol % chlorite and <5 vol % quartz. Plagioclase laths are partly replaced by a microcrystalline matrix of sericite, albite, calcite, epidote, and clinozoisite, forming pseudomorphs due to sericitization and saussuritization. Amphibole typically occurs as thin prisms and fibres of actinolite and tremolite,

replacing clinopyroxene. Clinopyroxene relicts occur as xenomorphic crystals surrounded by rims of actinolite. Clinozoisite forms idiomorphic crystals, whereas epidote is xenomorphic. Locally, igneous textures are well preserved and there is not a pervasive metamorphic fabric presented.

4.3.2. Metavolcanics

Metavolcanics are classified as metabasalts and metandesites. Metandesites display mainly porphyritic and interintersertal textures. They contain 40–60 vol % plagioclase, 5–10 vol % clinopyroxene, 5–10 vol % chlorite, 2–7 vol % amphibole and minor epidote, calcite, and quartz. Plagioclase form idiomorphic sericitized porphyrocrysts that are set in a fine-grained to microcrystalline matrix composed of allotriomorphic clinopyroxene relicts, epidote crystals, iron oxides, chlorite and devitrified glass (Figure 3e). Sporadic patches of interstitial quartz are common. Elongated veins filled with secondary minerals appear occasionally crosscutting the rock.

4.3.3. Serpentinized Harzburgites, Serpentinites

Serpentinized harzburgites show porphyroclastic texture with olivine constituting 50–70 vol %, orthopyroxene 15–30 vol %, and spinel up to 5 vol %. Olivine forms porphyroclasts as well as smaller polygonal neoblasts (~0.2 mm). The orthopyroxene forms isolated large crystals with lobate boundaries and often displays diopside exsollution lamellae, kink bands, and gliding parallel to (001). Minor clinopyroxene forms neoblastic grains in the recrystallized matrix. Dark-brown spinel forms disseminated anhedral crystals with lobate boundaries. The degree of serpentinization varies between 30% and 60%.

Serpentinites exhibit mesh textures. They consist essentially of serpentine minerals, mainly antigorite and chrysotile with minor chlorite, calcite, and talc. Occasionally relicts of olivine and Cr-spinel are presented. Pseudomorphic prismatic plates of bastite (lizardite pseudomorphs after pyroxenes), which sometimes mimic the cleavage of earlier pyroxene, are common. Sparsely, veinlets of calcite, serpentine, and talc crosscut the serpentinites.

4.4. Skyros

The collected metaophiolitic mafic and ultramafic rock samples from Skyros are classified as: (a) rodingites and (b) serpentinites.

4.4.1. Rodingites

Rodingites mainly display a blasto-subophitic texture with local relicts of primary subophitic texture, which is strongly indicative of a doleritic protolith (Figure 3f). They contain 30–50 vol % clinopyroxene, 20–30 vol % chlorite, 10–20 vol % garnet with minor calcite, titanite, and ilmenite. Clinopyroxene and chlorite formed probably after actinolite but they retain a crystal habit of an older clinopyroxene. Garnet (grossular) occurs in between the clinopyroxene grains and clearly pseudomorphs original plagioclase (Figure 3f). It comprises weakly birefringent, frequently tiny, micron-size crystals. Its small size and anisotropic character make it difficult to distinguish from vesuvianite, which also commonly appears in rodingites. Fe–Ti oxides with a dusty appearance are dispersed throughout the samples.

4.4.2. Serpentinites

The serpentinites are composed essentially of antigorite, chrysotile, and lizardite, with subordinate amounts of carbonates, chromite, magnetite, magnesite, talc, tremolite, and chlorite. Antigorite is the dominant mineral and occurs as interpenetrating and interlocking elongate plates. Sometimes, the antigorite flakes and blades are arranged in roughly parallel aggregates. Serpentine, which developed as an alteration after olivine, usually has a mesh texture while that formed after orthopyroxene has a bastite texture. These textures indicate dunite and harzburgite parent rocks.

The opaque minerals in the studied serpentinites are represented mainly by dark-brown spinel and magnetite. Spinel occurs as disseminated subhedral crystals and/or irregular grains. Alteration of spinel along grain borders and cracks is very common. Magnetite occurs as anhedral grains in the interstitial spaces between the serpentine minerals or as veinlets.

5. Whole-Rock Geochemistry

The chemical compositions of analyzed samples are presented in Table 1. Sample locations are indicated in Figure 2a–d. Standard geochemical diagrams have been utilized in order to classify the investigated former magmatic rocks (Figure 4).

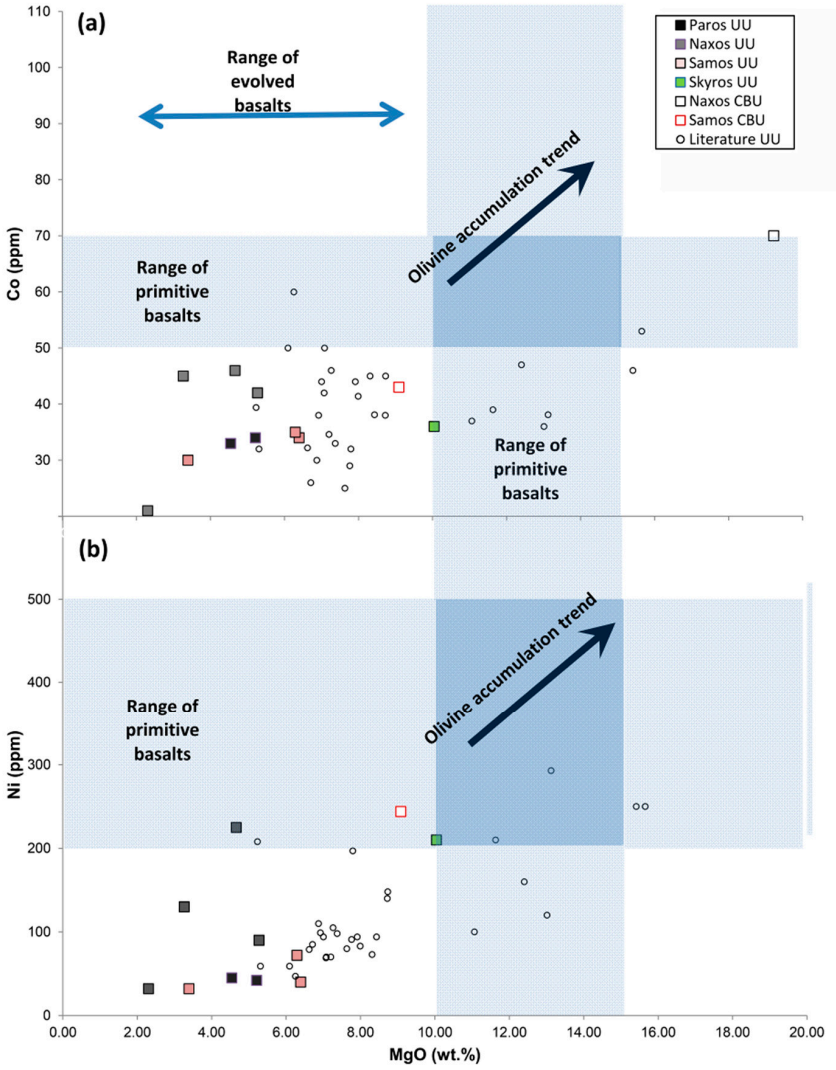

Figure 4. (**a**) MgO vs. Co and (**b**) MgO vs. Ni plot of Aegean metabasites. Upper Unit (UU) ophiolitic metabasites from the literature are also plotted: Ikaria ophiolitic mélange [10]; Tinos ophiolitic upper unit [15] (Mt. Tsiknias). Range expected for magmas in equilibrium with their mantle source: Ni: 200–500 ppm, Co: 50–70 ppm (from [49]). Naxos amphibolites (open squares) plot beyond the compositional range of the Figure 4a,b.

5.1. Upper Unit Metabasites

Studied ophiolitic metabasites from the Cycladic islands and Skyros span basalts, gabbros, and minor basaltic andesites and dolerites, ranging from 39 to 54.5 wt % SiO_2. Samples from the Cycladic

islands Paros, Naxos, and western Samos (Kallithea) include moderately to highly evolved basaltic rocks with 2.3 to 6.4 wt % MgO and Mg-number (Mg#) values from 40.2 to 59.6 (Figure 4) (Table 1). Only Skyros metabasites include primitive basaltic composition rocks with 10 wt % MgO at 50 wt % SiO_2, Ni > 200 ppm but Co < 50 ppm, thus indicating early olivine fractionation (Table 1) (Figure 4). TiO_2 contents of the relatively more primitive basaltic rocks (Paros: PA-9; Samos: SA-8, SA-2) are low, i.e., 0.6 to 0.7 wt % when compared to N- and E-type MORB compositions, and resemble typical island arc tholeiites or some Back-Arc Basin basalts, e.g., East Scotia (Table 1) [47,50]. In fact, there is a large range of TiO_2 content in the studied rocks that can be attributed to various processes, including fractionation and post-magmatic alteration.

A common feature in all the mafic rocks is the high potassium concentration. Even the less evolved rocks of gabbroic composition from Paros, SE Naoussa, contain up to 2 wt % K_2O (Table 1). Moreover, the Pb concentrations of all the Cycladic metabasites exceed 1 ppm (i.e., 1–17 ppm), which is high for typical MORB [51]. Notwithstanding, values up to 3 ppm may be normal for Back-Arc Basin basalts, e.g., in lavas from Southern Mariana Trough [52], yet most Cycladic rocks display extremely high values, up to 18 ppm, which clearly indicate secondary alteration (Table 1). The petrographic characteristics of the Cycladic metabasites (UU) document ocean-floor hydrothermal alteration (hydration), especially associated with extensive sericitization of plagioclase, which justifies the mobility of alkalis and lead. This is further attested in the spread of $^{207}Pb/^{206}Pb$ diagram (see Section 5.4).

Few detailed studies have been made of the Cycladic upper unit metabasites and the discussion in this section is based on the dataset of [15] on Tinos metagabbros (UU) and Ikaria ophiolitic rocks (Faros mélange) [10]. In order to elucidate the petrogenesis of the Cycladic rocks, we rely on the relatively immobile key elements. The Total Akali-Silica (TAS) proxy diagram of [51] is considered to provide an effective discrimination of altered ophiolitic rocks, avoiding the wide dispersion of the IUGS TAS [53,54]. The Nb/Y ratio is used as a proxy for total alkalis ($Na_2O + K_2O$) and Zr/Ti as a proxy for SiO_2. In Figure 5 most Cycladic metabasites span the field of tholeiiteic basalts and basaltic andesites. A group of samples from the Naxos Upper Unit (metabasalts, basaltic andesites) and two amphibolites from Ikaria plot in the field of alkali basalts (Nb/Y > 1). Sample SA-8 (meta-andesite) plot as an outlier due to extremely high Nb/Y value (7.85), indicating extreme alkalinity of the magma and possibly a different magmatic type.

High precision Zr-Y determinations are a particularly sensitive method of distinguishing different magma batches in a magmatic suite. Both elements remain essentially incompatible within basaltic magma during fractional crystallization. Hence, a single magma batch will retain an almost constant Y/Zr ratio [42]. In Figure 6a there is a reasonable linear correlation between Zr and Y but the Zr/Y ratio is variable. The majority of upper unit metabasites exhibit mainly a tholeiitic affinity (one linear trend), whereas a small group of samples from Naxos shows a different linear trend with higher Zr/Y (e.g., 5.2–5.4). Such relationship cannot be attributed to crystallization of a single magma batch. Similar geochemical systematics have been reported from the sheeted dyke suite and pillow lavas of Troodos complex [42] and basalts from modern Back-Arc Basins [55].

The V–Ti plot (Figure 6b) of [56] is used for further tectonic-magmatic classification of ophiolites from suprasubduction zones, and is considered here to investigate the main ophiolite complexes of the Western Ophiolite Belt (Pindos: [57]; E. Othrys: [58]; Gevgeli: [59]). This diagram (Figure 6b) also shows the spectrum of magmatic affinities recognised above: (a) MORB tholeiites and (b) island arc tholeiite affinities (Paros and western Samos-Kallithea); (c) boninitic affinities (high-MgO, low-TiO_2 andesites and gabbros) displayed by Skyros.

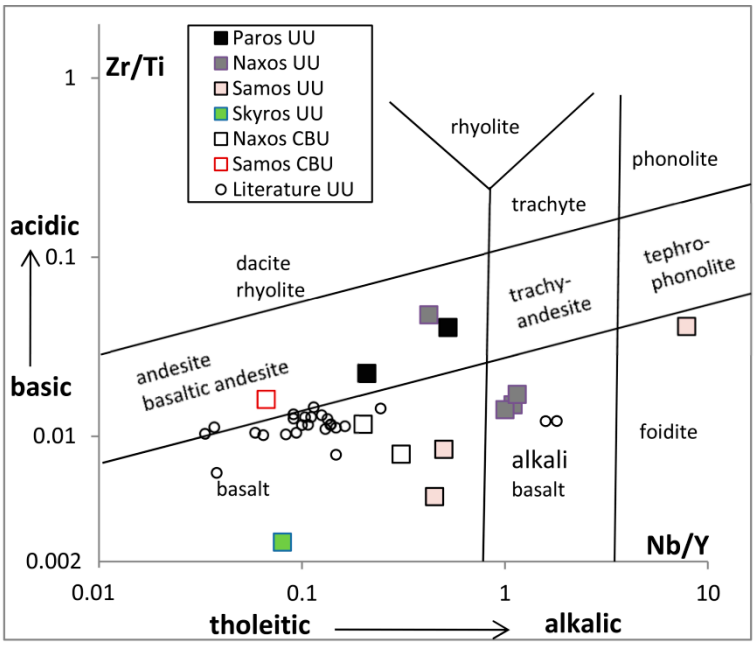

Figure 5. Classification of Aegean ophiolitic metabasites using the immobile element-based TAS proxy diagram (modified after [53,54]). Literature data for Upper Unit metabasites are plotted for comparison (see text).

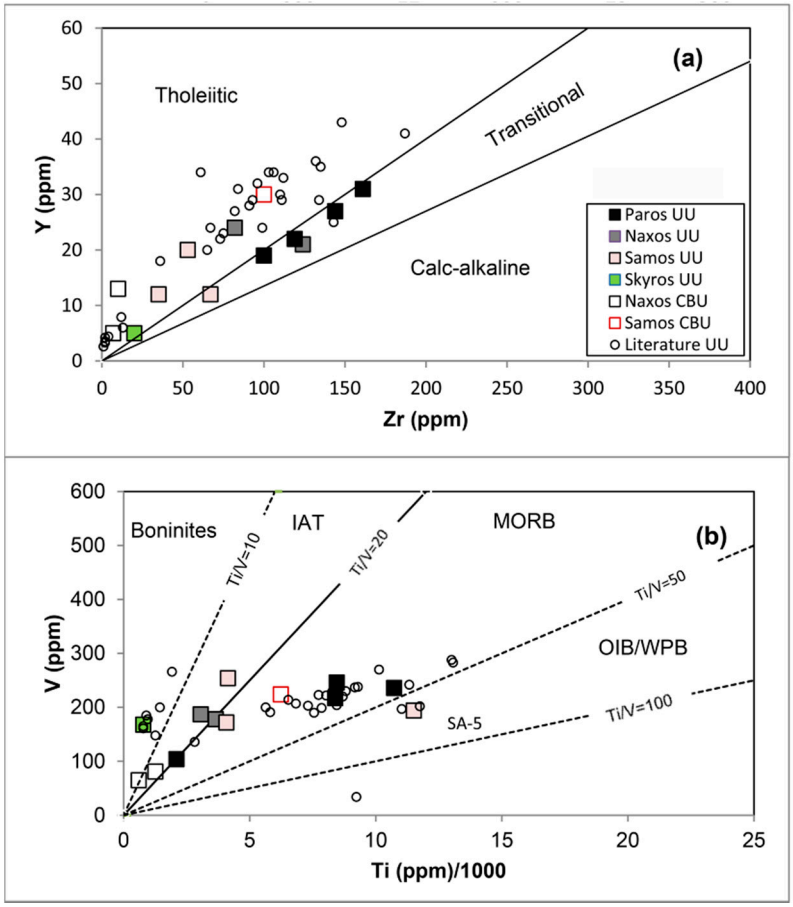

Figure 6. (**a**) Zr vs. Y and (**b**) Ti vs. V [56] tectonic-magmatic discrimination of Cycladic ophiolitic metabasites.

5.2. Naxos Amphibolites and Central Samos Metagabbro (CBU)

Two amphibolite samples from the Naxos gneiss dome (NA-7: Kourounohori, NA-9: Agia) show very low TiO_2 contents (TiO_2: 0.1–0.2 wt %) and extremely high MgO (19–27 wt %) for mafic rocks, and very low Al_2O_3 at $SiO_2 \geq 52\%$ (Table 1). According to the extreme composition of this group of rocks and considering the microscopic observations of thin sections, NA-9 ampibolite is interpreted as a metamorphosed tholeiitic basalt, whereas NA-7 is probably a metasomatised cummulate rock, in particular a former pyroxenite (NA-7). The bulk-rock geochemical characteristics of these amphibolites are comparable to amphibolites from metamorphic soles beneath the ultramafic ophiolites in northern Evia [8]. A metagabbro (SA-11) from a metamorphosed ophiolitic mélange in central Samos-Myli, displays primitive basaltic composition with 9 wt % MgO at 50.3 wt % SiO_2. Ni and Co contents of the latter sample is lower than 250 ppm and 50 ppm, respectively, thus indicating early olivine fractionation [49] (Figure 4a,b). In Figure 6, SA-11 metagabbro plots in the field of MORB tholeiites whereas Naxos amphibolites plot in the field of island arc tholeiites.

5.3. Multi-Element Geochemical Patterns

For representation of multi-element spider diagram patterns (Figure 7), only immobile elements are included and ordered in increasing compatibility, in the standard form after [51]. Typical compositions of basaltic rocks from modern well defined settings are shown for direct comparisons. In general, relatively immobile elements under seafloor hydrothermal alteration of oceanic crust are considered the High-Field-Strength Element (HFSE) group (e.g., Zr, Nb, Ta, Ti), the REEs, Mg, Y, and especially the transition metals (Sc, V, Cr, Fe, Co, Ni, and Zn) [60,61]. On the contrary, the Large Ion Lithophile Elements (LILE) K, Rb, Ba, Sr, and U are considered readily mobile under low-temperature alteration of ocean floor basalts and basaltic glass, and they are commonly added through the process of the formation of clay [62,63].

In these diagrams, N-type MORB [48] is selected as a normalized factor because the resulting flat N-MORB pattern is a useful reference regarding tectonic setting.

The Cycladic samples can be classified into three geochemical groups (Figure 7a–g):

(a) Paros metagabbros (Figure 7a) (SE Naoussa—Upper Unit) and Samos (Kallithea nappe) metavolcanites (Figure 7b) display a Zr-Y flat pattern and higher Th/Y ratio relative to MORB or OIB; these characteristics are typical of modern arc lavas from complex tectonic settings (C-MORB, Taitao lavas, Chile; [51] and references therein). The gradient of the patterns for the Paros-W. Samos samples is even higher than that for back-arc basin basalts (BABB) tholeiites (Figure 7a,b). Moreover, the $(La/Nb)_N$ ratios, which range from 1.2 to 2.35 (Figure 6b), emphasize the HFSE depletion of this type of magmas relative to LREE, which is another characteristic feature of arc magmas [64,65].

(b) Sample SA-11 (metagabbro from CBU), from central Samos, displays a flat pattern typical for MORB (Figure 7b). Following the definition of N-type MORB of [66], this sample exhibits Ce/Nb > 2.5 but $Ce_N/Yb_N = 1$ (Table 1) and, combined with initial Sr > 0.7035, it is assigned to an enriched MORB category (E-MORB) rather than N-MORB. However, comparing sample SA-11 with a complete dataset from [15] (Figure 7f) it becomes clear that there is a whole range of compositions typical of BABB, similar to Troodos ophiolitic lavas [51].

(c) Trace element patterns of Naxos metabasaltic rocks (NA-3, NA-15) share many characteristics with oceanic island basalts (OIB) (Figure 7c): low Zr/Nb (i.e., ~5) relative to N-MORB [67], high Nb/Y, and the negative gradient in the Ti–Yb(Y) part of the diagram, which are characteristics of enriched ocean-island basalts (OIB). This is distinct from the flat patterns for Ti–Yb(Y) that characterize both N- and EMORB compositions.

(d) Naxos amphibolites (CBU) also display a high Th/Y ratio similar to Paros and western Samos metabasalts; however, they also have a strong depletion for most of the trace elements LREE and HFSE, compared to typical MORB patterns (Figure 7c).

(e) Skyros metagabbro shows a typical pattern of boninitic rocks (Figure 7d) from modern oceanic arc environments, such as the fore-arc volcanics of the Mariana-Izu-Bonin [68]. One metabasalts and a metagabbro from the same area also show similar boninitic affinities (data from [41], Table 1).

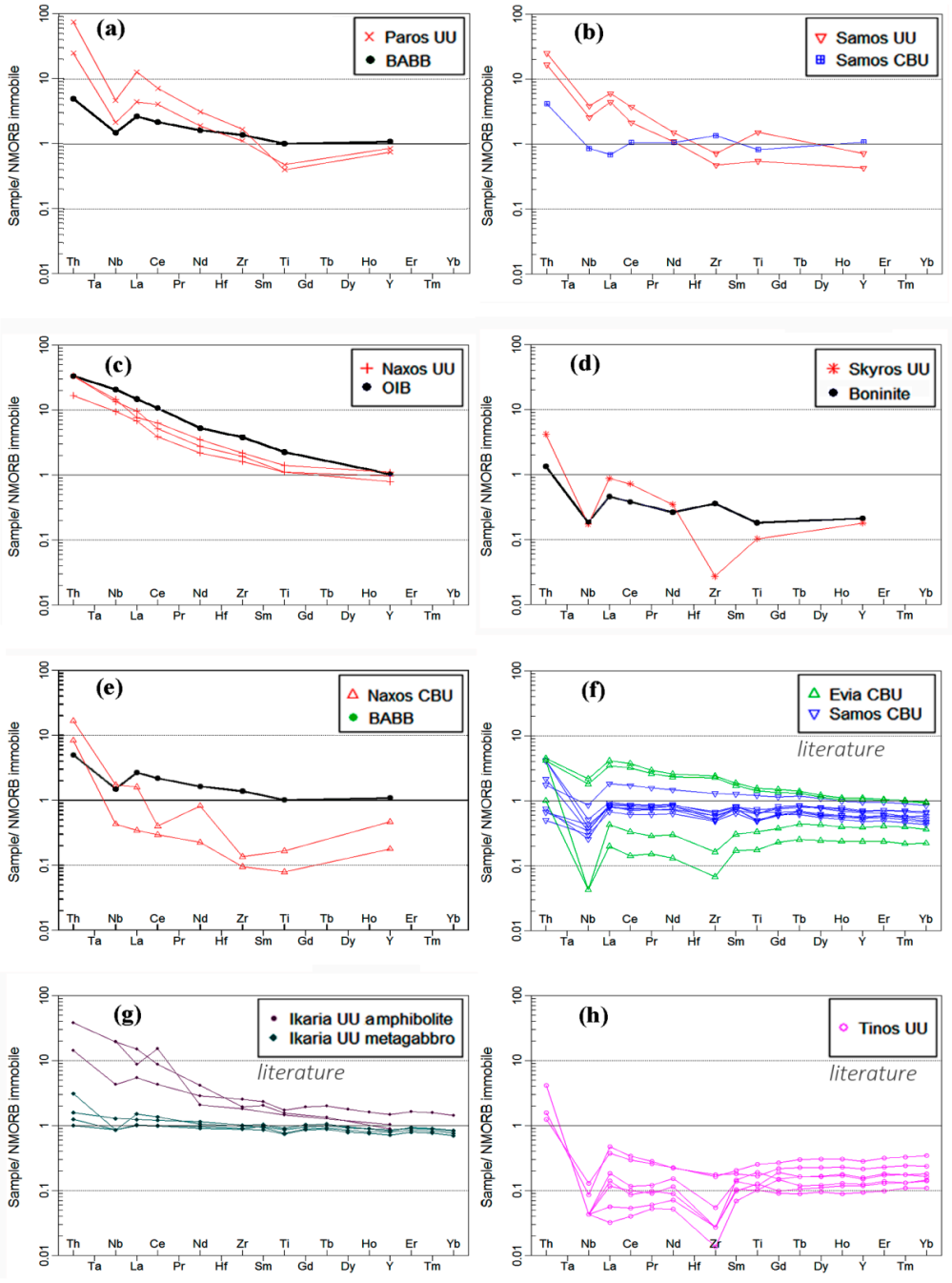

Figure 7. Incompatible, immobile element patterns (spidergrams) for Aegean ophiolites along with some typical basaltic compositions from different tectonic setting. Data sources, see [51] and references in the text; BABB from [52]; Boninite from [66]. Normalisation is to N-MORB [51]. (**a**) Paros; (**b**) western Samos-Kallithea nappe and central Samos (CBU) metagabbros; (**c**) Naxos metabasalts (UU); (**d**) Skyros metadolerite (SK-1); (**e**) Naxos amphibolites (CBU) from the flanks of the gneiss dome; (**f**) central Samos CBU) and southern Evia (CBU) metagabbros from [15]; (**g**) Ikaria upper unit (Faros and Kefala units from [10]); (**h**) Tinos-Mt Tsiknias (Upper Unit) metagabbros from [15].

5.4. Upper Unit Serpentinites and Serpentinized Peridotites

Major and trace element contents of 20 representative samples from Cyclades and Skyros have been analyzed and the results are listed in Table 1.

a. Cycladic serpentinites

Based on the olivine-orthopyroxene-clinopyroxene CIPW normative classification, most of the Cycladic serpentinite protoliths are assigned to harzburgites and minor olivine orthopyroxenite whereas only one sample from Skyros (SK-9) is assigned to the lherzolite category. However, published data for metaperidotites from the main horizon of Naxos gneiss dome [29] (Katzir et al., 1999) display a broader compostional range from lherzolites to harzburgites and rare dunites, whose variability is not shown in the upper unit peridotites of Naxos possibly due to the scattered occurrence of the upper unit serpentinites (Figure 8). In major element variation diagrams the Mg# is used as a fractionation index (Figure 9a–c). The Mg# values are high in all the Cycladic rocks, ranging from 84 to 91.5. SiO_2, Al_2O_3, and CaO display negative correlation trends defined by the Paros-Naxos peridotites, which are similar to those found for the main horizon of metaperidotites from Naxos. These trends have been attributed to a successive depletion process caused by melt extraction from an original lherzolitic mantle source as indicated in Figure 9d [29]. In the binary diagram of MgO/SiO_2 vs. Al_2O_3/SiO_2 (Figure 9d), the serpentinized peridotites and serpentinites of our study plot below the "successive magmatic depletion" line, as expected for moderately serpentinized peridotitic rocks [69–71], which is attributed to restricted loss of Mg during seafloor weathering after serpentinization [71,72]. The Aegean serpentinites are comparable to peridotites of the western ophiolite belt (e.g., east Othris [73].

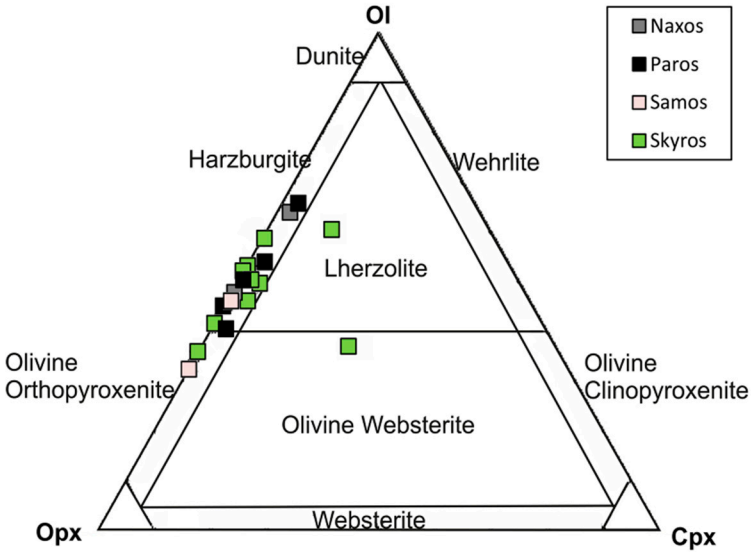

Figure 8. Spinel peridotite norm compositions of the ultramafic rocks from the Cyclades and Skyros plotted on the ultramafic classification diagram of IUGS.

Compositional variation of the Cycladic serpentinites show a dominant chemical group with average low Al_2O_3 (0.3–1.5 wt %), TiO_2 (0.01–0.04 wt %) and CaO (0.03–1.52 wt %), and low V (5–49 ppm), coupled with high Ni (2318 ppm), Co (81–123 ppm), and Cr (1935–3932 ppm), indicating a highly residual nature of the mantle source; they are comparable to the composition of harzburgites from Pindos ophiolite complex [74] and mantle wedge serpentinites from oceanic fore-arc settings [75] (Figure 9). A subordinate group from Paros-Naxos displays a relatively less refractory character testified by the higher Al_2O_3 (1.79–2.86 wt %) and V (50–60 ppm), and lower Co (96–103 ppm) and Cr (2398–2677 ppm) concentrations. Two serpentinite samples, one from Samos (SA-14) and one from

Skyros (SK-4), display unusually high Al_2O_3 values of 4.82 and 8.61, respectively (Figure 9b). Based on thin section observations and mineral analysis data, these values can be attributed to extensive chlorite intergrowth in serpentine.

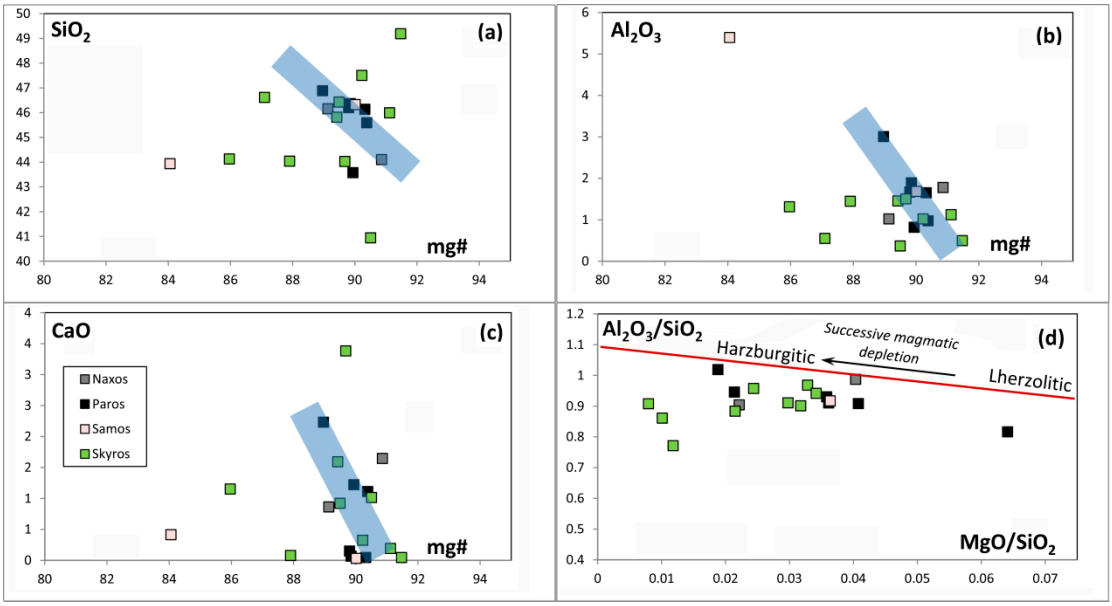

Figure 9. Variation diagrams of (**a**) SiO_2; (**b**) Al_2O_3 and (**c**) CaO vs. Mg# as fractionation index for the Aegean ultramafic rocks; (**d**) Binary diagram of Mg/SiO_2 vs. Al_2O_3/SiO_2 with serpentinized peridotites and serpentinites. Successive magmatic depletion line according to [69–71]. The shaded field shows the main magmatic trend defined by Paros samples. Skyros serpentinites display the largest scatter, due to alteration effects.

b. Skyros serpentinites

Skyros serpentinites are classified mostly as hartzburgites, except from one sample as lherzolite and another as olivine websterite (Figure 8). Skyros ultramafic rocks display the highest Mg# (up to 91.5). Ni and Cr abundances are as high as 2720 ppm and 3932 ppm, respectively.

5.5. Sr-Nd Results

Sr and Nd isotope ratios were determined for 12 samples. The three peridotite samples failed to produce Nd isotopic data due the very low content of REEs (<1 ppm). The results are summarized in Table 2 and presented in Figure 10a,b. Initial Sr and εNd values have been recalculated at 160 Ma, which corresponds to the available mean ages of the Pindos Jurassic ophiolite, and at 80 Ma, for the case of metaigneous rocks from the CBU [15,76–78]. The Cycladic ophiolites exhibit initial $^{143}Nd/^{144}Nd$ values lower than 0.5130, which is the lower limit value of most N-type middle ocean ridge basalts (N-type MORB), and higher initial $^{87}Sr/^{86}Sr$ ratios than 0.7035 [66]. These isotopic values, if primary, suggest that the source of these rocks was isotopically modified from an enriched mantle component (OIB). Generally, the initial Sr-Nd isotopic ratios of Cycladic metabasites display a large scatter considering the number of samples analyzed. In the Sr-Nd isotopic diagram of Figure 10a, a main, horizontal trend is recognized. This trend is defined by the metamorphosed gabbros of central Samos (CBU), and sample SA-11 (Myli location, this study) also plot along this trend together with a serpentinite from Samos and the Tinos (UU) metagabbros (Mt. Tsiknias) [15]. This trend is characterized by a shift towards higher $^{87}Sr/^{86}Sr$ (ISr80 = 0.7062 to 0.708) at almost constant initial $^{143}Nd/^{144}Nd$ (εNd80 = +6.54 to +7.48), calculated for a presumed protolith age of 80 Ma. The Skyros metadolerite (SK-1) also plots together with the Samos and Tinos metabasites. In Figure 10b initial isotopic ratios are recalculated at 160 Ma

which is the approximate age of the Pindos ophiolite complex ([77]; and references therein]). In the latter diagram, Paros (PA-9) and Naxos (NA-3) upper unit metabasites plot close to Avdella mélange gabbros, and define a separate group showing elevated initial Sr (0.70413–0.70563) and distinctly lower εNd (+4.13–+0.32) isotopic values compared to the Samos field. Sr and Nd isotope compositions of metagabbros from Andros CBU (calculated for 160 Ma) can be clearly distinguished from the other Cycladic metabasites (Paros, Naxos, Tinos) samples by even higher $^{87}Sr/^{86}Sr$ = 0.70613 to 0.70694 ratios and lower εNd = −3.77 to −1.54 values (Figure 10b), strongly indicating significant crustal involvement from terrigenous sediment or arc crust [15,28].

Upper Unit ophiolites of Paros and Naxos show a strong coupling of the two isotopic systems towards more radiogenic Sr and less radiogenic Nd isotopic ratios. This second trend could possibly be attributed to the combined effect of contamination of the source from a subduction-derived component (hydrous fluids or melt) and seafloor hydrothermal alteration.

5.6. Lead Isotope Geochemistry

Lead isotopes, in combination with other isotopic systems (Sr-Nd), have been proven as an important source of information on the source reservoir of magmatic rocks [79]. In this study, lead isotope compositions were measured on samples from metavolcanites and metagabbros from the Upper and intermediate Units of the Cyclades. Lead isotope compositions of the metabasites are given in Table 3.

The analyzed metabasites from the Cyclades (metagabbros, metabasalts, and metabasaltic andesites) display a wide range of lead isotope compositions for a relatively small number of samples, especially regarding $^{207}Pb/^{204}Pb$ ratios ($^{206}Pb/^{204}Pb$ = 18.40–21.53; $^{207}Pb/^{204}Pb$ = 15.56–15.77; $^{208}Pb/^{204}Pb$ = 38.32–39.6) [80] (Figure 11a,b). Similarly, high whole-rock $^{207}Pb/^{204}Pb$ ratios (Figure 11a) have been reported for the hydrothermally altered parts of the Troodos ophiolite complex (greenschists and epidosites) [80]. In the ^{207}Pb-^{206}Pb and ^{208}Pb-^{206}Pb diagrams, the Cycladic metabasites display a spread beyond the normal MORB field and Troodos glasses [80] and plot within the field of seawater, attesting the effect of seawater alteration on the Cycladic metabasites compositions. Sample NA-14 (serpentinized harzburgite) has a high $^{206}Pb/^{204}Pb$ ratio, probably due to time-integrated development of radiogenic lead caused by a higher U/Pb ratio compared to the other samples (not plotted in Figure 11).

Table 2. Rb-Sr and Sm-Nd isotope data of representative ophiolitic metabasites and serpentinites from the Aegean islands of Paros, Naxos, Samos, and Skyros.

Sample No.	Rock Type	Rb	Sr	$^{87}Rb/^{86}Sr$	$^{87}Sr/^{86}Sr$ (m)	2σ	$^{87}Sr/^{86}Sr$ (80 Ma)	$^{87}Sr/^{86}Sr$ (160 Ma)
Metabasites								
NA-3	Metabasalt	79	206	1.1098	0.706656	0.000004	0.705395	0.704132
NA-9	Amphibolite	8	33	0.7018	0.710557	0.000009	0.709759	0.708961
PA-9	Metagabbro	56	299	0.5420	0.706858	0.000015	0.706242	0.705625
SA-8	Metandesite	101	50	5.8454	0.705731	0.000004	0.707109	0.692435
SA-11	Metagabbro	62	259	0.6928	0.707224	0.000004	0.706437	0.705648
SK-1	Metadorerit.	8	116	0.1996	0.707165	0.000006	0.706938	0.706711
Serpentinites								
NA-6	Dunite	1	5	0.5262	0.707540	0.000013	0.706942	0.706343
NA-14	Serpentinite	2	6	0.9045	0.708138	0.000011	0.707109	0.706078
PA-7	Serpentinite	2	5	1.0584	0.708772	0.000016	0.707569	0.706364
PA-16	Serpentinite	1	47	0.0610	0.709102	0.000004	0.709033	0.708964
SA-12	Serpentinite	2	3	1.6571	0.709911	0.000100	0.708034	0.706155
SK-4	Serpentinite	2	12	0.6212	0.708550	0.000023	0.707847	0.707143

Table 2. *Cont.*

Sample No.	Rock Type	Sm	Nd	$^{147}Sm/^{144}Nd$	$^{143}Nd/^{144}Nd$ (m)	2σ	εNd (CHUR) (0 Ma)	$^{143}Nd/^{144}Nd$ (80 Ma)	$\varepsilon Nd_{(CHUR)}$ (80 Ma) *	$^{143}Nd/^{144}Nd$ (160 Ma)	$\varepsilon Nd_{(CHUR)}$ (160 Ma)
Metabasites											
NA-3	Metabasalt	6	26	0.136990	0.512786	0.000005	2.91	0.512715	3.52	0.512644	4.13
NA-9	Amphibolite	bdl	2	-	0.512406	0.000020	−4.51	-	-	-	-
PA-9	Metagabbro	3	14	0.136890	0.512592	0.000004	−0.90	0.512520	−0.29	0.512449	0.32
SA-8	Metandesite	2.8	13	0.130253	0.512689	0.000003	1.01	0.512622	1.69	0.512554	2.37
SA-11	Metagabbro	3	8	0.253171	0.513000	0.000008	7.07	0.512868	6.49	0.512735	5.91
SK-1	Metadorerit.	bdl	3	-	0.512932	0.000018	5.75	-	-	-	-
Serpentinites											
NA-6	Dunite	n.d	n.d	-	-	-	-	-	-	-	-
NA-14	Serpentinite	n.d	n.d	-	-	-	-	-	-	-	-
PA-7	Serpentinite	n.d	n.d	-	0.512710	0.000062	1.41	-	-	-	-
PA-16	Serpentinite	n.d	n.d	-	-	-	-	-	-	-	-
SA-12	Serpentinite	bdl	2	-	0.512990	0.000041	6.87	-	-	-	-
SK-4	Serpentinite	2	11	0.104920	0.512240	0.000005	−7.76	0.512185	−6.83	0.512130	−5.89

n.d: not detected, bdl: below detection limit. * 80 Ma is the reported age of Samos metagabbros from [15]. $^{87}Rb/^{86}Sr$ and $^{147}Sm/^{144}Nd$ isotopic ratios were calculated on the basis of whole rock Rb/Sr and Sm/Nd ratios (concentrations from XRF analysis), using the applications of GCDKit 4.0 software [81] and equations of [82]. Initial isotopic ratios and epsilon Nd values were calculated using the plug-in modules of GCDKit software.

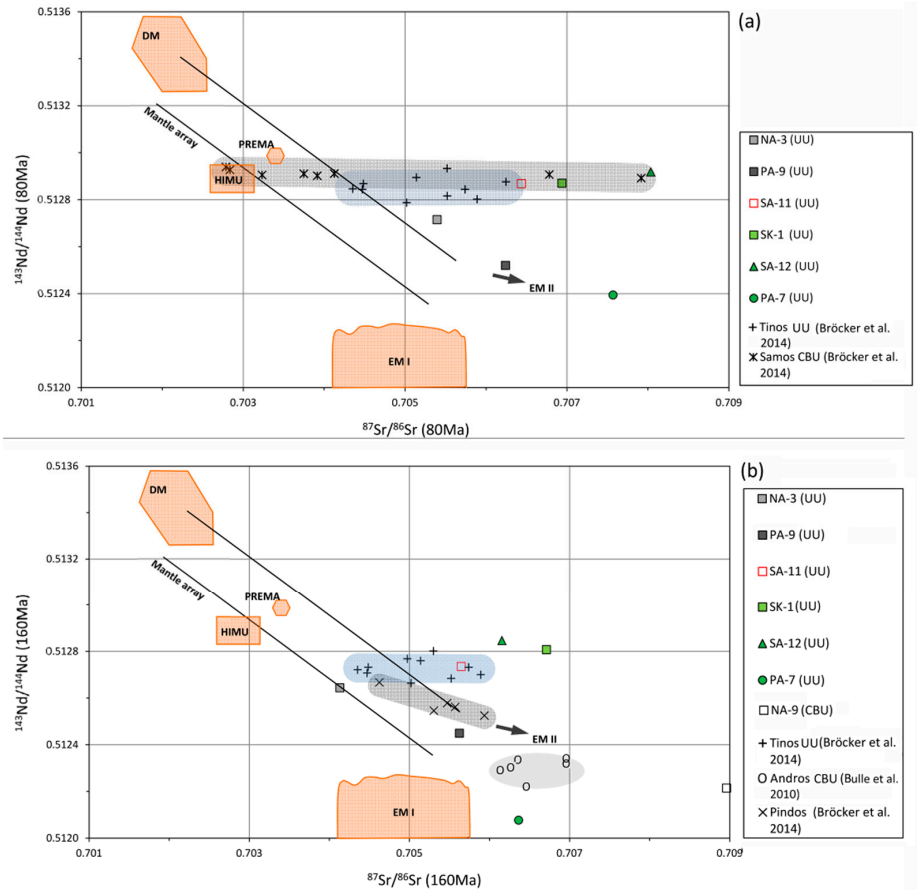

Figure 10. Sr–Nd isotope compositions of mafic rocks from the Upper Units of Naxos, Paros, Samos (Kallithea), and Skyros and Naxos amphibolites, also showing data from the HP-mélange blocks from central Samos, Tinos, and a Pindos-Avdella melange [15,28]. (**a**) $^{87}Sr/^{86}Sr$ vs. $^{143}Nd/^{144}Nd$ plot for age recalculation t = 80 Ma; schematic fields of comparison indicated by abbreviations: N-MORB = Normal type Mid-Ocean Ridge Basalt; OIB = Ocean-Island basalt; IAB = Island Arc Basalt; (**b**) $^{87}Sr/^{86}Sr$ vs. $^{143}Nd/^{144}Nd$ plot with ratios calculated for t = 160 Ma. Terrestrial mantle reservoirs: DMM, HIMU, PREMA, EM-I, EM-II from [69].

Table 3. Lead isotope compositions of ophiolitic metabasites and associated serpentinites from the Aegean islands (NA—Naxos, SA—Samos).

Sample No.	NA-3	NA-9	SA-8	SA-11	NA-6	NA-14
Rock Type	**Metabasalt**	**Amphibolite**	**Metabasalt**	**Metabasalt**	**Serp. Harzb.**	**Serp. Harzb.**
$^{206}Pb/^{204}Pb$	18.802	18.816	18.670	18.703	18.518	21.534
$^{207}Pb/^{204}Pb$	15.625	15.771	15.607	15.665	15.594	15.838
$^{208}Pb/^{204}Pb$	39.039	39.065	38.807	38.799	38.419	38.326

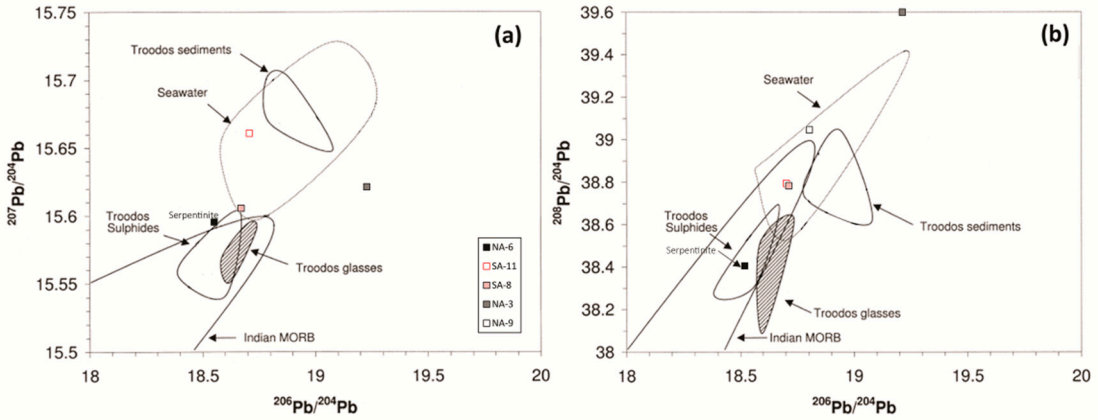

Figure 11. (**a**) $^{208}Pb/^{204}Pb$ versus $^{206}Pb/^{204}Pb$ and (**b**) $^{207}Pb/^{204}Pb$ versus $^{206}Pb/^{204}Pb$ plots showing the isotopic compositions of the Cycladic metabasites. Fields for Troodos glasses, sulfides, sediments, and seawater form [80] and references therein.

6. Discussion

6.1. Determining the Effect of Alteration on the Cycladic Metabasites

In general, the Cycladic metabasites exhibit K enrichment when compared to gabbroic rocks from recent oceanic crust. For instance, normal MORB compositions do not exceed 0.17 wt % K_2O (e.g., [79]. This enrichment in K_2O is attributed to an addition of potassium (plus Rb and Pb) due to low-T seafloor alteration reactions in basalts, which is commonly observed within the oceanic crust ([83]; and references therein]). Sericitization of plagioclase is a common feature in all the mafic lithotypes (metagbbros and metavolcanites). Similar K-enrichments are reported in gabbroic rocks and dolerite dykes from southern Aegean ophiolites (Crete, Rhodes, and Karpathos [21]).

Moreover, the $^{87}Sr/^{86}Sr$ ratio is considered a very powerful indicator of hydrothermal alteration in the oceanic crust, whereby fresh modern crust is unradiogenic ($^{87}Sr/^{86}Sr$ = 0.7025–0.703) and modern seawater is radiogenic (0.7092) [79]. Based on microscopic observations (e.g., Figure 3a) and the formation of secondary minerals, all the Cycladic upper unit samples show evidence of low-temperature seafloor hydrothermal alteration at greenschist facies. Sr-Nd isotopic variations of Samos (and Tinos, data from [28]) samples display a characteristic shift towards higher $^{87}Sr/^{86}Sr$ (up to 0.708) at almost constant initial $^{143}Nd/^{144}Nd$ (i.e., εNd_{80} = +6.54 to +7.48) (Figure 10). This shift indicates a seawater contribution at hydrothermal conditions of upper extrusive oceanic crust, and is a common feature in Mediterranean ophiolite complexes (e.g., Troodos: [83]). Previous authors [83] suggested that interchange of Jurassic and Cretaceous seawater Sr with ocean crust Sr occurs during hydrothermal circulation and may buffer the Sr isotope composition of seawater. Nevertheless, seawater $^{87}Sr/^{86}Sr$ has changed with time; thus, before 80 My, seawater was less radiogenic (0.7076) than today and has increased since then [84,85]. The value of 0.708 is the maximum value of $^{87}Sr/^{86}Sr$ found in the Cycladic metabasites. In this context, the initial $^{87}Sr/^{86}Sr$ of the metabasites reflects the mixing ratio of seawater-derived Sr and basalt Sr present in a sample. Thus,

the significance of Sr isotope values for determining the characteristics of the magmatic protolith and tectonic setting is limited. From Figure 11a,b it is clear that the Pb-isotopic ratios for Samos and Naxos metabasites show wide variation, from close to MORB into the seawater field. The elevated $^{207}Pb/^{206}Pb$ and the large scatter of values, which overlaps with the seawater, also suggest that the Pb incorporated in the Cycladic metabasites is derived from the seawater. The positive correlation between $^{206}Pb/^{204}Pb$ and $^{208}Pb/^{204}Pb$ for all the Cycladic rocks (serpentinite-metagabbros-metabasalts) is attributed to the mixing relationships between the magmatic and seawater end-member components (hydrothermal system).

6.2. Comparisons of the Upper Unit and CBU Ophiolites of the Broader Aegean Region

The geochemical characteristics of the Upper Unit ophiolites reveal significant differences between the Cycladic rocks (Paros-Naxos-Western Samos) and Skyros:

(a) Random occurrence of ophiolitic lithologies characterizes the Cycladic mélange units, whereas the Skyros ophiolite consists of more coherent slices of metabasites with essentially boninitic affinities.

(b) Basalts with Ocean Island type (OIB) affinities and alkaline characteristics are recognized in the Cycladic islands (Naxos-Ikaria), but are also common elsewhere in the Cycladic belt and the mainland ophiolite complexes: the amphibolite soles of central–northern Evia ophiolite [8] and Ikaria [10], as well as the main Western Ophiolite Belt (Avdella mélange-Pindos and Koziakas: [86]). These rocks display extreme HFSE enrichments relative to N-type MORB (high Ti, P and Nb, Zr/Y ~5, Nb/Y > 1). Alkaline basalts (AB) found in ophiolites mainly include rocks formed at seamounts (OIB) [87]. They mainly occur as tectonic slices or blocks incorporated into mélanges, that is, as accreted fragments of oceanic terranes. Contrary to the Pindos peridotites, the Cycladic rocks exhibit variable enrichments in alkali earth elements (Sr, Rb, and Ba). These enrichments are a common feature of the Cycladic serpentinites from mélange units, which have been interpreted in different ways: oceanic hydrothermal alteration, synmetamorphic fluid–rock interaction, igneous differentiation, or some combination of these processes (e.g., S. Evia, Syros: [17,34]). Due to the random variation in these mobile elements (Sr, Rb, and Ba) we consider these enrichments a result of ocean floor hydrothermal alteration.

(c) The peridotite relicts in Cycladic ophiolites display considerable chemical and petrographic variation and a general refractory nature. Overall their composition correlates with the two groups distinguished by [74] for the ultramafic rocks of the Pindos complex. The observed elemental variations are typical of serpentinites corresponding to harzburgites from mantle wedge settings (Supra Subduction Zones—SSZ [75]).

There is a scarcity of ages for the formation of metaophiolites from the upper unit of the Cycladic islands (Paros, Naxos, and western Samos) and the broader Aegean region. In most cases, available ages are based on isotopic data for metamorphic soles and on paleontological data of closely associated sediments (e.g., [18] and references therein). Due to that fact, regional correlations between the remnant ophiolitic occurrences exposed in the mélange units of the CBU and the upper unit are difficult to establish. Only for a few ophiolite occurrences ion probe U–Pb zircon ages have been reported [15,76,77]. In terms of geochemical characteristics, previous work revealed mid-ocean ridge to island arc affinities (e.g., metagabbros and glaucophanites) from Syros, Tinos, and adjacent islands, and this observation has been interpreted to indicate a back-arc setting [88,89].

6.3. Regional Correlation and Significance

A regional correlation of Cycladic metabasites from upper unit ophiolite mélanges and CBU mélanges is attempted (a total of 60 analyses) in order to examine possible clustering of compositions. Published data include the supra-detachment mélange units of Ikaria (Faros and Kefala: [10]), Tinos Upper Unit (Mt Tsiknias: [15]), which can be directly correlated to the low-pressure ophiolitic

mélange units of the present study. The metaophiolitic mélanges (within CBU) include S. Andros (Late Jurassic), S. Evia (undated), central Samos-Selcuk nappe, and Tinos CBU (Late Createous) [15,28]).

A combination of discriminant plots have been used to examine the diversity of magma types and refine their tectonic setting. In the Zr vs. Zr/Y discriminant plot (Figure 12a) [60], the Zr/Y ratio is used against Zr as a fractionation index, to investigate long term source heterogeneities and distinguish between basalts erupted in within-plate settings, mid-ocean ridges or volcanic arcs. In Figure 12a the Zr vs. Zr/Y systematics (Figure 12a) suggests that the distribution of geochemical groups is random between the upper unit and CBU. Three magmatic types are recognized: normal MORB, Volcanic Arc Basalts (VAB) and Within Plate Basalts (WPB). Skyros and Tinos (Upper Unit) metagabbros (Figure 12a) define a separate field and plot together with Tethyan ophiolite boninitic lavas, late dykes and the Mariana Fore Arc Basalts fall [57].

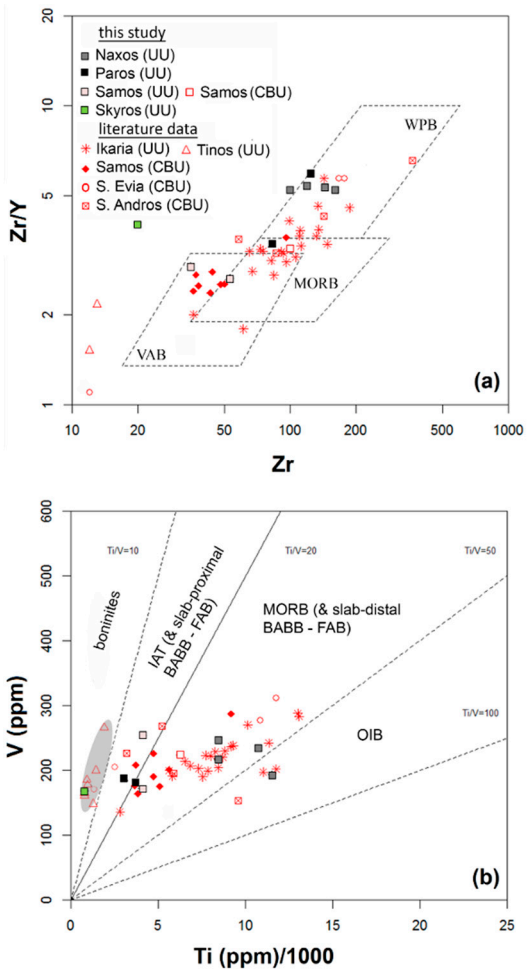

Figure 12. Tectonomagmatic discrimination of metabasites (gabbros, basaltic andesites, and dolerites) of Aegean ophiolites: (**a**) Zr vs. Zr/Y [60], and (**b**) Ti/V discriminant plot of [56] modified in field names after [50]. Abbreviations in (**a**): VAB = Volcanic Arc Basalt, WPB = Within-Plate Basalt and MORB = Mid-Ocean Ridge Basalt; in (**b**): OIB = Ocean Island Basalt, IAT = Island Arc Tholeiite; FAB = Fore-Arc Basalt, BABB = Back-Arc Basin Basalts. Symbols: black = this study, red = published data (data from Samos, Tinos Upper Unit, S. Evia: [15]; Andros: [28]; Ikaria: [10]).

True MORB samples are only a few, the majority of Cycladic metabasites plot in the transitional VAB/MORB field. From the WPB group, only Naxos metabasalts, and two amphibolite samples from Ikaria (Faros) [10], can be geochemically classified as alkali basalt: Nb/Y > 1 and high P, Ba, Sr and Ce_N/Yb_N, higher than E-MORB (i.e., >2) these geochemical features rather resemble OIB-type

(see Table 1). Alkali basalts are very commonly associated with tholeiitic rocks in many Mesozoic Tethyan ophiolite mélanges in the Hellenides, and were mostly interpreted as remnants of intra-oceanic islands (OIB) or sea-mounts in the Pindos ocean (Pindos-Avdella: [74], Koziakas: [86]). Alkali basalts in modern oceanic setting are associated with fractures zones, seamounts, and aseismic ridges [50].

The V–Ti discriminant plot of [56] is considered to provide further information for distinguishing between ophiolites already recognized as having a suprasubduction zone origin [51]. Based on Ti vs. V relationships (Figure 12b), the Skyros and Tinos (Upper Unit) metagabbros have very low Ti and exhibit arc-like Ti/V <10. These rocks plot in the same area of late stage boninitic basalts and basaltic andesite dykes of the Pindos-Mirdita ophiolite complexes [57,74]. In this diagram (Figure 12b) Paros and Andros and part of Samos metagabbros exhibit arc-like Ti/V = 10–20; however, most of Cycladic rocks plot within the broad field of mid-ocean ridge basalts (MORB) and back-arc basin basalts (BABB): Ti/V = 20–50.

Previous work on the HP mélanges from the NW Cycladic islands (Syros: [32]; Sifnos: [89]) revealed a similar complicated range of magmatic types in metagabbros and glaucophanites: mid-ocean ridge to island arc affinities. This observation has been interpreted to indicate a transition from subduction initiation to back-arc spreading magmatism (e.g., Tinos, Syros: [28,88]; Sifnos: [89]).

6.4. Tectonic Setting

Extensive geochronological dating (U-Pb on zircons) and geochemical studies have focused on metagabbros and felsic gneisses within mélange units [15,17,28,90,91] and the marble-schist sequences of the CBU [76,91]. Previous studies have shown, on the basis of δO^{18} and εHf values of zircons, that Late Cretaceous igneous zircons (Syros and Tinos: [76,87,90,91]) are characterized by MORB-like affinities, suggesting that the Late Cretaceous magmas were produced by partial melting of depleted MORB mantle. Fu et al. [91] also pointed out the significant crustal component in 160 Ma metagabbros from Andros, implying that some Jurassic gabbroic rocks of the Hellenides are not part of SSZ-type (supra-subduction zone) ophiolites that are common elsewhere along the margin of the Pelagonian zone (Western Ophiolite belt).

So far, both harzburgite compositions and those of metabasites (gabbros and dolerites) are linked by the fact that their chemical affinities share many characteristics with supra-subduction zone setting magmatism [66,92].

7. Conclusions

The results of this study can be summarized as follows:

(a) Metavolcanics (dolerites, basaltic andesites, minor basalts) and metagabbros from all the upper unit ophiolitic exposures exhibit wide ranges of major element composition (SiO_2: 39–56.6 wt %; Mg-number: 37.5–69.2 and high K_2O i.e., >0.2 wt %), indicating derivation from evolved magmas.

(b) The petrographic, major and trace element and Sr-isotope data show that all the studied rocks (metagabbros, metavolcanics, and peridotites) underwent ocean floor alteration. Microscopic observations corroborate that low-temperature alteration during the generation of the ocean crust affected the upper unit metavolcanites and metagabbros.

(c) Based on the immobile- element TAS proxy classification diagram, Ti/V, Zr/Y vs. Zr discriminant plots and spidergram patterns of N-MORB-normalized compositions, three magmatic groups are recognized among the upper unit (UU) ophiolitic metabasites: (i) metabasites from Paros and western Samos (Kallithea melange) display affinities of island arc tholeiites (IAT); (ii) Naxos basaltic rocks are highly enriched in incompatible elements and display an OIB type affinity, representing an oceanic island setting; (iii) Metagabbros from the northern Skyros ophiolitic-mélange (Fere-Kambos) and Tinos (Upper Unit—Mt. Tsiknias) exhibit boninitic affinities indicating a fore-arc setting.

(d) Central Samos metagabbros of the Cycladic Blueschists Unit (CBU) are primitive rocks with Back-Arc Basin affinities.

(e) Most peridotite relicts from Samos, Paros, and Naxos—irrespective of the structural unit—display common chemical affinities similar to ocean floor peridotites formed in a supra-subduction zone environment. Major and trace element characteristics of harzburgite relicts in Cycladic serpentinites and Skyros indicate a highly residual nature of the mantle source, comparable to the mantle wedge serpentinites from oceanic fore-arc settings, in accordance with previous studies.

(f) A combination of Pb and Sr isotopic characteristics of the Cycladic metabasites shows the importance of seawater hydrothermal alteration on the composition of the studied metaophiolitic rocks. Trace element patterns of Central Samos metabasites (CBU) and Nd isotopes suggest affinities of Back-Arc Basin Basalts (BABB).

Supplementary Materials: The following are available online at www.mdpi.com/2076-3263/7/1/14/s1. Supplementary Table S1 provides information about sample locations, tectonic units, and rock types. Moreover, detailed description for the XRF analyses is documented in Supplementary Document 1.

Acknowledgments: The University of Leicester provided the XRF and microprobe analytical facilities. We thank the authors of the GCDkit software (Vojtěch Janušek, Colin M. Farrow and Vojta Erban) for providing the free software with which geochemical plots were prepared. National and Kapodistrian University of Athens is acknowledged for supporting this work. We would like to thank Konstantinos Soukis for valuable information and discussions on the structural relationships of the ophiolite exposures with the main tectonic units in the Cyclades. Two anonymous reviewers are kindly thanked for their constructive criticism that led to the improvement of previous versions of this manuscript.

Author Contributions: This paper is partly based on unpublished data from the PhD thesis of Iakovos Pantziris, National and Kapodistrian University of Athens, Geology Department; the research work was designed and supervised by professor Panagiotis Mitropoulos who conceived all the experimental work; Iakovos Pantziris performed the sampling and most of the whole rock analytical experiments; Christos Kanellopoulos, Robert Moritz and Massimo Chiaradia performed the isotopic analyses, at the University of Geneva. Panagiotis Pomonis accomplished the petrography work; Charalampos Vasilatos, Christina Stouraiti and Panagiotis Pomonis analyzed the data and made the graphical presentation and the interpretation of the results; Christina Stouraiti wrote the paper.

Conflicts of Interest: The authors declare no conflict of interest.

References

1. Dürr, S.; Altherr, R.; Keller, J.; Okrusch, M.; Seidel, E. The median Aegean crystalline belt: Stratigraphy, structure, metamorphism, magmatism. In *Alps, Apennines, Hellenides*; Closs, H., Roeder, D.H., Schmidt, K., Eds.; IUGS Report; Schweizerbart: Stuttgart, Germany, 1978; Volume 38, pp. 455–477.
2. Altherr, R.; Kreuzer, H.; Wendt, I.; Lenz, H.; Wagner, G.A.; Keller, J.; Harre, W.; Höhndorf, A.A. Late Oligocene/Early Miocene high temperature belt in the Attic–Cycladic belt in the Attic–Cycladic crystalline complex (SE Pelagonian, Greece). *Geol. Jahrb.* **1982**, *23*, 97–164.
3. Patzak, M.L.; Okrusch, M.; Kreuzer, H. The Akrotiri unit on the island of Tinos, Cyclades, Greece: Witness to a lost terrane of Late Cretaceous age. *Neues Jahrb. Geol. Paläontol.* **1994**, *194*, 211–252.
4. Katzir, Y.; Matthews, A.; Garfunkel, Z.; Schliestedt, M. The tectonometamorphic evolution of a dismembered ophiolite (Tinos, Cyclades, Greece). *Geol. Mag.* **1996**, *133*, 237–254. [CrossRef]
5. Pe-Piper, G.; Piper, D.J.W. *The Igneous Rocks of Greece. The Anatomy of an Orogeny*; Schweizerbart: Stuttgart Germany, 2002; 573p.
6. Soukis, K.; Stockli, D. Structural and thermochronometric evidence for multi-stage exhumation of southern Syros, Cycladic islands, Greece. *Tectonophysics* **2013**, *595–596*, 148–164.
7. Robertson, A.H.F.; Shallo, M. Mesozoic-Tertiary evolution of Albania in its regional Eastern Mediterranean context. *Tectonophysics* **2000**, *316*, 197–254. [CrossRef]
8. Gartzos, E.; Dietrch, V.J.; Migiros, G.; Serelis, K.; Lymperopoulou, T. The origin of amphibolites from the metamorphic soles beneath the ultramafic ophiolites in Evia and Lesvos (Greece) and their geotectonic implication. *Lithos* **2009**, *108*, 224–242. [CrossRef]

9. Jolivet, L.; Menant, A.; Sternai, P.; Rabillard, A.; Arbaret, L.; Augier, R.; Laurent, V.; Beaudoin, A.; Grasemann, B.; Huet, B.; et al. The geological signature of a slab tear below the Aegean. *Tectonophysics* **2015**, *659*, 166–182. [CrossRef]
10. Pe-Piper, G.; Photiades, A. Geochemical characteristics of the Cretaceous ophiolitic rocks of Ikaria island Greece. *Geol. Mag.* **2006**, *143*, 417–429. [CrossRef]
11. Pomonis, P.; Hatzipanagiotou, K. Petrography and geochemistry of relict peridotites of the Kallithea-Drakei area (W. Samos). *Bull. Geol. Soc. Greece* **1998**, *32*, 215–224.
12. Jolivet, L.; Brun, J.-P. Cenozoic geodynamic evolution of the Aegean. *Int. J. Earth Sci.* **2010**, *99*, 109–138. [CrossRef]
13. Malandri, C.; Soukis, K.; Maffione, M.; Özkaptan, M.; Vassilakis, E.; Lozios, S.; van Hinsbergen, D.J.J. Vertical-axis rotations accommodated along the Mid-Cycladic lineament on Paros Island in the extensional heart of the Aegean orocline (Greece). *Lithosphere* **2016**. [CrossRef]
14. Bargnesi, E.A.; Stockli, D.F.; Mancktelow, N.; Soukis, K. Miocene core complex development and coeval supradetachment basin evolution of Paros, Greece, insights from (U–Th)/He thermochronometry. *Tectonophysics* **2013**, *595–596*, 165–182.
15. Bröcker, M.; Löwena, K.; Rodionov, N. Unraveling protolith ages of meta-gabbros from Samos and the Attic–Cycladic Crystalline Belt, Greece: Results of a U–Pb zircon and Sr–Nd whole rock study. *Lithos* **2014**, *198–199*, 234–248.
16. Katzir, Y.; Garfunkel, Z.; Avigad, D.; Matthews, A. The geodynamic evolution of the Alpine orogen in the Cyclades (Aegean Sea, Greece): Insights from diverse origins and modes of emplacement of ultramafic rocks. In *The Geodynamics of the Aegean and Anatolia*; Taymaz, T., Yilmaz, Y., Dilek, Y., Eds.; Geol. Soc. London Spec. Publ., The Geological Society of London: London, UK, 2007; Volume 291, pp. 17–40.
17. Bröcker, M.; Enders, M. Unusual bulk-rock compositions in eclogite-facies rocks from Syros and Tinos (Cyclades, Greece): Implications for U-Pb zircon geochronology. *Chem. Geol.* **2001**, *175*, 581–603. [CrossRef]
18. Robertson, A.H.F. Overview of the genesis and emplacement of Mesozoic ophiolites in the Eastern Mediterranean Tethyan region. *Lithos* **2002**, *65*, 1–67. [CrossRef]
19. Papanikolaou, D. Timing of tectonic emplacement of the ophiolites and terrane paleogeography in the Hellenides. *Lithos* **2009**, *108*, 262–280. [CrossRef]
20. Robertson, A.H.F. Late Palaeozoic–Cenozoic tectonic development of Greece and Albania in the context of alternative reconstructions of Tethys in the Eastern Mediterranean region. *Int. Geol. Rev.* **2012**, *54*, 373–454. [CrossRef]
21. Rassios, A.; Smith, A.G. Constraints on the formation and emplacement age of western Greece ophiolites (Vourinos, Pindos and Othris) inferred from deformation structures in peridotites. In *Ophiolites and Ocean Crust: New Insights from Field Studies and the Ocean Drilling Program*; Dilek, Y., Moores, E.M., Elthon, D., Nicolas, A., Eds.; Geological Society of America Special Papers; The Geological Society of America: Boulder, CO, USA, 2000; pp. 473–483.
22. Jacobshagen, V.; Dürr, S.; Kockel, E.; Kopp, K.O.; Kowalczyk, G. Structure and geodynamic evolution of the Aegean region. In *Alps, Appenines, Hellenides*; Closs, H., Roeder, D., Schmid, K., Eds.; E. Schweitzerbartsche Verlagsbuchhandlung: Stuttgart, Germany, 1978; pp. 537–564.
23. Wakabayashi, J.; Dilek, Y. What constitutes' emplacement of an ophiolite? Mechanisms and relationship to subduction initiation and formation of metamorphic soles. In *Ophiolites in Earth History*; Dilek, Y., Robinson, P.T., Eds.; Geol. Soc. London Spec. Publ., The Geological Society of London: London, UK, 2003; Volume 218, pp. 427–447.
24. Dilek, Y.; Furnes, H. Ophiolites and their origin. *Elements* **2014**, *10*, 93–100.
25. Vanderhaeghe, O. Structural development of the Naxos migmatite dome. In *Gneiss Domes in Orogeny*; Whitney, D.L., Teyssier, C., Siddoway, C.S., Eds.; The Geological Society of America: Boulder, CO, USA, 2004; pp. 211–227.
26. Theodoropoulos, D. Geological map of Greece, 1:50,000, Samos Island. Institute of Geology and Mineral Exploration: Athens, Greece, 1979.
27. Papantoniou, G. The Structure and History of the Strike—Slip Fault Zone of Skyros Island, Central—North Aegean. Master's Thesis, National and Kapodistrian University of Athens, Athens, Greece, 2015.
28. Bulle, F.; Bröcker, M.; Gärtner, C.; Keasling, A. Geochemistry and geochronology of HP mélanges from Tinos and Andros, Cycladic Blueschist Belt, Greece. *Lithos* **2010**, *117*, 61–81. [CrossRef]

29. Katzir, Y.; Avigad, D.; Matthews, A.; Garfunkel, Z.; Evans, B.W. Origin and metamorphism of ultrabasic rocks associated with continental margin, Naxos (Cyclades, Greece). *J. Metamorph. Geol.* **1999**, *17*, 301–318. [CrossRef]
30. Pantziris, I. Geochemical—Petrological Study of Basic—Ultrabasic Rocks from the Aegean Islands. Ph.D. Thesis, National and Kapodistrian University of Athens, Athens, Greece, 2000.
31. Okrusch, M.; Bröcker, M. Eclogite facies rocks in the Cycladic Blueschist Belt, Greece: A review. *Eur. J. Mineral.* **1990**, *2*, 451–478.
32. Bröcker, M.; Franz, L. The base of the Cycladic Blueschist Unit on Tinos Island (Greece) re-visited: Field relationships, phengite chemistry and Rb–Sr geochronology. *Neues Jahrb. Mineral. Abh.* **2005**, *181*, 81–93.
33. Bröcker, M.; Franz, L. Dating metamorphism and tectonic juxtaposition on Andros Island (Cyclades, Greece): Results of a Rb–Sr study. *Geol. Mag.* **2006**, *143*, 609–620. [CrossRef]
34. Katzir, Y.; Matthews, A.; Garfunkel, Z.; Evans, B.W. Origin, HP/LT metamorphism and cooling of ophiolitic mélanges in southern Evia (NW Cyclades) Greece. *J. Metamorph. Geol.* **2000**, *18*, 699–718. [CrossRef]
35. Bröcker, M.; Kreuzer, H.; Matthews, A.; Okrusch, M. $^{40}Ar/^{39}Ar$ and oxygen isotope studies of polymetamorphism from Tinos Island Cycladic blueschist belt, Greece. *J. Metamorph. Geol.* **1993**, *11*, 223–240. [CrossRef]
36. Tomaschek, F.; Kennedy, A.K.; Villa, I.M.; Lagos, M.; Ballhaus, C. Zircons from Syros, Cyclades, Greece—Recrystallization and mobilization of zircon during high pressure metamorphism. *J. Petrol.* **2003**, *44*, 1977–2002. [CrossRef]
37. Gautier, P.; Brun, J.P.; Moriceau, R.; Sokoutis, D.; Martinod, J.; Jolivet, L. Timing, kinematics and cause of Aegean extension: A scenario based on a comparison with simple analogue experiments. *Tectonophysics* **1999**, *315*, 31–72. [CrossRef]
38. Baziotis, I.; Mposkos, E. Origin of metabasites from upper tectonic unit of the Lavrion area (SE Attica, Greece): Geochemical implications for dual origin with distinct provenance of blueschist and greenschist's protoliths. *Lithos* **2011**, *126*, 161–173. [CrossRef]
39. Bröcker, M.; Pidgeon, R.T. Protolith ages of meta-igneous and meta-tuffaceous rocks from the Cycladic Blueschist Unit, Greece: Results of a reconnaissance U–Pb zircon study. *J. Geol.* **2007**, *115*, 83–98. [CrossRef]
40. Ring, U.; Gessner, K.; Güngör, T.; Passchier, C.W. The Menderes massif of western Turkey and the Cycladic massif in the Aegean: Do they really correlate? *J. Geol. Soc. Lond.* **1999**, *156*, 3–6. [CrossRef]
41. Karkalis, C.; Magganas, A.; Koutovitis, P. Petrological, mineralogical and geochemical data of Eohellenic ophiolitic rocks in the island of Skyros, Greece. *Bull. Geol. Soc. Greece* **2016**, *50*, 1867–1877.
42. Tarney, J.; Marsh, N.G. Major and trace elements geochemistry of Holes CY-1 and CY-4: Implications for petrogenetic models. In *Cyprus Crustal Study Project; Initial Report, Holes CY-1 and 1a*; Gibson, I.L., Mapas, J., Robinson, P.T., Xenophontos, C., Eds.; Paper No. 90-20; Geological Survey of Canada: Ottawa, ON, Canada, 1992; pp. 133–175.
43. Pin, C.; Briot, D.; Bassin, C.; Poitrasson, F. Concomitant separation of strontium and samarium-neodymium for isotopic analysis in silicate samples, based on specific extraction chromatography. *Anal. Chim. Act.* **1994**, *298*, 209–217. [CrossRef]
44. Tanaka, T.; Togashi, S.; Kamioka, H.; Amakawa, H.; Kagami, H.; Hamamoto, T.; Yuhara, M.; Orihashi, Y.; Yoneda, S.; Shimizu, H.; et al. JNdi-1: A neodymium isotopic reference in consistency with LaJolla neodymium. *Chem. Geol.* **2000**, *168*, 279–281. [CrossRef]
45. Baker, J.; Peate, D.; Waight, T.; Meyzen, C. Pb isotopic analysis of standards and samples using a ^{207}Pb-^{204}Pb double spike and thallium to correct for mass bias with a double-focusing MC-ICPMS. *Chem. Geol.* **2004**, *211*, 275–303. [CrossRef]
46. McArthur, J.M.; Howarth, R.J.; Bailey, T.R. Strontium isotope stratigraphy: LOWESS version 3: best fit to the marine Sr-isotope curve for 0–509 Ma and accompanying look-up table for deriving numerical age. *J. Geol.* **2001**, *109*, 155–169.
47. Luff, I.W. Petrogenesis of the island arc tholeiite series of the South Sandwich islands. Ph.D. thesis, University of Leeds, Leeds, UK, 1982.
48. Sun, S.S.; McDonough, W.F. Chemical and isotopic systematics of oceanic basalts: Implications for mantle composition and processes. In *Magmatism in Ocean Basins*; Saunders, A.D., Norry, M., Eds.; Geol. Soc. London Spec. Publ., The Geological Society of London: London, UK, 1989; Volume 42, pp. 313–345.

49. Merle, R.; Marzoli, A.; Reisberg, L.; Bertrand, H.; Nemchin, A.; Chiaradia, M.; Callegaro, S.; Jourdan, F.; Bellieni, G.; Kontak, D.; et al. Sr, Nd, Pb and Os isotope systematics of CAMP tholeiites from Eastern North America (ENA): Evidence of a subduction-enriched mantle source. *J. Petrol.* **2013**, *55*, 133–180. [CrossRef]
50. Wilson, M. *Igneous Petrogenesis*; Unwin Hyman: London, UK, 1989; p. 232.
51. Pearce, J.A. Immobile element fingerprinting of ophiolites. *Elements* **2014**, *10*, 101–108. [CrossRef]
52. Pearce, J.; Stern, R.; Bloomer, S.; Fryer, P. Geochemical mapping of the Mariana arc-basin system: Implications for the nature and distribution of subduction Component. *Geochem. Geophys. Geosyst.* **2005**, 6. [CrossRef]
53. Pearce, J.A. A user's guide to basalt discrimination diagrams. *Geol. Assoc. Can. Spec. Publ.* **1996**, *12*, 79–113.
54. Floyd, P.A.; Winchester, J.A. Magma type and tectonic setting discrimination using immobile elements. *Earth Planet. Sc. Lett.* **1975**, *27*, 211–218. [CrossRef]
55. Pearce, J.; Stern, R. Origin of Back-Arc Basin Magmas: Trace Element and Isotope Perspectives. In *Back-Arc Spreading Systems: Geological, Biological, Chemical, and Physical Interactions*; Christie, D.M., Fisher, C.R., Lee, S.-M., Givens, S., Eds.; Geophysical Monograph Series, 166; American Geophysical Union: Washington DC, USA, 2006; pp. 63–86.
56. Shervais, J.W. Ti-V plots and the petrogenesis of modern and ophiolitic lavas. *Earth Planet. Sci. Lett.* **1982**, *59*, 101–118. [CrossRef]
57. Whattam, S.A.; Stern, R.J. The subduction initiation rule: A key for linking ophiolites, intra-oceanic forearcs and subduction initiation. *Contrib. Mineral. Petrol.* **2011**, *162*, 1031–1045. [CrossRef]
58. Koutsovitis, P. Gabbroic rocks in ophiolitic occurrences from East Othris, Greece: Petrogenetic processes and geotectonic environment implications. *Mineral. Petrol.* **2012**, *104*, 249–265. [CrossRef]
59. Saccani, E.; Photiades, A. Mid-ocean ridge and supra-subduction affinities in the Pindos ophiolites (Greece): Implications for magma genesis in a forearc setting. *Lithos* **2004**, *73*, 229–253. [CrossRef]
60. Pearce, J.A.; Norry, M.J. Petrogenetic implications of Ti, Zr, Y and Nb variations in volcanic rocks. *Contrib. Mineral. Petrol.* **1979**, *69*, 33–47. [CrossRef]
61. Saunders, A.D.; Tarney, J.; Marsh, N.G.; Wood, D.A. Ophiolites as ocean crust or marginal basin crust: A geochemical approach. In *Ophiolites, Proceedings of the International Ophiolite Symposium*; Panayiotou, A., Ed.; Ministry of Agriculture and Natural Resources, Geological Survey Department: Nicosia, Cyprus, 1980; pp. 193–204.
62. Gills, K.M.; Robinson, P.T. Distribution of alteration zones in the upper oceanic crust. *Geology* **1988**, *16*, 262–266. [CrossRef]
63. Staudigel, H. Chemical fluxes from hydrothermal alteration of the oceanic crust. In *Treatise on Geochemistry*, 2nd ed.; Turekian, K.K., Holland, H.D., Eds.; Elsevier: London, UK, 2014; Volume 4, pp. 583–606.
64. Hastie, A.R.; Ramsook, R.; Mitchell, S.F.; Kerr, A.C.; Millar, I.L.; Darren, F. Geochemistry of Compositionally Distinct Late Cretaceous Back-Arc Basin Lavas: Implications for the Tectonomagmatic Evolution of the Caribbean Plate. *J. Geol.* **2010**, *118*, 655–676. [CrossRef]
65. Perfit, M.R.; Gust, D.A.; Bence, R.; Arculus, J.; Taylor, S. Chemical characteristics of island arc basalts: Implications for mantle sources. *Chem Geol.* **1980**, *30*, 227–256.
66. Saunders, A.D.; Norry, M.J.; Tarney, J. Origin of MORB and chemically-depleted mantle reservoirs: Trace element constraints. *J. Petrol. Spec. Lithosph. Issue* **1988**, *1*, 415–445. [CrossRef]
67. Wood, D.A.; Joron, J.L.; Treuil, M. A re-appraisal of the use of trace elements to classify and discriminate between magma series and different tectonic settings. *Earth Planet. Sc. Lett.* **1979**, *45*, 326–336. [CrossRef]
68. Reagan, M.K.; Ishizuka, O.; Stern, R.J.; Kelley, K.A.; Ohara, Y.; Blichert-Toft, J.; Bloomer, S.H.; Cash, J.; Fryer, P.; Hanan, B.B.; et al. Fore-arc basalts and subduction initiation in the Izu-Bonin-Mariana system. *Geochem. Geophys.* **2010**, *11*, Q03X12. [CrossRef]
69. Zindler, A.; Hart, S. Chemical Geodynamics. *Annu. Rev. Earth Planet. Sci.* **1986**, *14*, 493–571. [CrossRef]
70. Niu, Y. Bulk-rock major and trace element compositions of abyssal peridotites: Implications for mantle melting, melt extraction and post-melting processes beneath mid-ocean ridges. *J. Petrol.* **2004**, *45*, 2423–2458. [CrossRef]
71. Boschi, C.; Bonatti, E.; Ligi, M.; Brunelli, D.; Dallai, L.; D'Orazio, M.; Fróh-Green, G.L.; Tonarini, S.; Barnes, J.; Bedini, R. Serpentinization of mantle peridotites along an uplifted lithospheric section, Mid Atlantic Ridge at 11° N. *Lithos* **2013**, *178*, 3–23. [CrossRef]
72. Snow, J.E.; Dick, H.J.B. Pervasive magnesium loss by marine weathering of peridotite. *Geochim. Cosmochim. Acta* **1995**, *59*, 4219–4235. [CrossRef]

73. Magganas, A.; Koutsovitis, P. Composition, melting and evolution of the upper mantle beneath the Jurassic Pindos Ocean inferred by ophiolitic ultramafic rocks in East Othris, Greece. *Int. J. Earth Sci.* **2015**, *104*, 1185–1207. [CrossRef]
74. Saccani, E.; Photiades, A. Petrogenesis and tectono-magmatic significance of volcanic and subvolcanic rocks in the Albanide-Hellenide ophiolitic mélanges. *Isl. Arc* **2005**, *14*, 494–516. [CrossRef]
75. Deschamps, F.; Godard, M.; Guillot, S.; Hattori, K. Geochemistry of subduction zone serpentinites: A review. *Lithos* **2013**, *178*, 96–127. [CrossRef]
76. Bröcker, M.; Keasling, A. Ionprobe U-Pb zircon ages from the high-pressure/low-temperature mèlange of Syros, Greece: Age diversity and the importance of pre-Eocene subduction. *J. Metamorph. Geol.* **2006**, *24*, 615–631. [CrossRef]
77. Liati, A.; Gebauer, D.; Fanning, C.M. The age of ophiolitic rocks of the Hellenides (Vourinos, Pindos, Crete): First U–Pb ion microprobe (SHRIMP) zircon ages. *Chem. Geol.* **2004**, *207*, 171–188. [CrossRef]
78. Parlak, O.; Karaoğlan, F.; Rızaoğlu, T.; Klötzli, U.; Koller, F.; Billor, Z. U–Pb and ^{40}Ar–^{39}Ar geochronology of the ophiolites and granitoids from the Tauride belt: Implications for the evolution of the Inner Tauride suture. *J. Geodyn.* **2013**, *62*, 22–37. [CrossRef]
79. White, W.M.; Klein, E.M. Composition of the oceanic crust. In *Treatise on Geochemistry*, 2nd ed.; Holland, H.D., Turekian, K.K., Eds.; Elsevier: Amsterdam, The Netherlands, 2014; pp. 457–496.
80. Booij, E.; Bettison-Varga, L.; Farthing, D.; Staudigel, H. Pb-isotope systematics of a fossil hydrothermal system from the Troodos ophiolite, Cyprus: Evidence for a polyphased alteration history. *Geochim. Cosmochim. Acta* **2000**, *64*, 3559–3569. [CrossRef]
81. Janousek, V.; Farrow, C.M.; Erban, V. Interpretation of whole-rock geochemical data in igneous geochemistry: Introducing Geochemical Data Toolkit (GCDkit). *J. Petrol.* **2006**, *47*, 1255–1259. [CrossRef]
82. Faure, G. *Principles of Isotope Geology*, 2nd ed.; John Wiley & Sons: New York, NY, USA, 1986; p. 589.
83. Spooner, E.T.C.; Fyfe, W.S. Sub-sea-floor metamorphism, heat and mass transfer. *Contrib. Mineral. Petrol.* **1973**, *42*, 287–304. [CrossRef]
84. Richter, F.M.; Rowley, D.B.; DePaolo, D.J. Sr isotope evolution of seawater: The role of tectonics. *Earth Planet. Sci. Lett.* **1992**, *109*, 11–23. [CrossRef]
85. Veizer, J. Strontium isotopes in seawater through time. *Annu. Rev. Earth Planet. Sci.* **1989**, *17*, 141–167. [CrossRef]
86. Pomonis, P.; Tsikouras, B.; Hatzipanagiotou, K. Petrogenetic evolution of the Koziakas ophiolite complex, (W. Thessaly, Greece). *Mineral. Petrol.* **2007**, *89*, 77–111.
87. Saccani, E. A new method of discriminating different types of post-Archean ophiolitic basalts and their tectonic significance using Th-Nb and Ce-Dy-Yb systematics. *Geosci. Front.* **2015**, *6*, 481–501. [CrossRef]
88. Seck, H.A.; Kötz, J.; Okrusch, M.; Seidel, E.; Stosch, H.G. Geochemistry of a meta-ophiolite suite: An association of metagabbros, eclogites and glaucophanites on the island of Syros, Greece. *Eur. J. Mineral.* **1996**, *8*, 607–623.
89. Moçek, B. Geochemical evidence for arc-type volcanism in the Aegean Sea: The blueschist unit of Siphnos, Cyclades (Greece). *Lithos* **2001**, *57*, 263–289. [CrossRef]
90. Fu, B.; Paul, B.; Cliff, J.; Bröcker, M.; Bulle, F. O-Hf isotope constraints on the origin of zircons in high-pressure melange blocks and associated matrix rocks from Tinos and Syros, Greece. *Eur. J. Mineral.* **2012**, *24*, 277–287. [CrossRef]
91. Fu, B.; Bröcker, M.; Ireland, T. Zircon U–Pb, O, and Hf isotopic constraints on Mesozoic magmatism in the Cyclades, Aegean Sea, Greece. *Int. J. Earth Sci.* **2015**, *104*, 75–87. [CrossRef]
92. Weaver, B.L.; Wood, D.A.; Tarney, J.; Joron, J.L. Geochemistry of ocean island basalts from the south Atlantic: Ascension, Bouvet, St. Helena, Gough and Tristan da Cunha. In *Alkaline Igneous Rocks*; Fitton, J.G., Upton, B.G.J., Eds.; Geol. Soc. London Spec. Publ., The Geological Society of London: London, UK, 1987; Volume 30, pp. 253–267.